Chapter 2

Fabrication and Characterization of p-Si/n-TiO_2 Heterojunction Diodes Grown by Sol-Gel and E-Beam Evaporation Methods for Optical Application

2.1 Introduction

It has been discussed in Chapter-1 that p-Si/n-TiO_2 thin film (TF) based heterojunctions have drawn considerable attention for UV detection [Zhang *et al.* (2012-c), Chakrabartty *et al.* (2014)], gas sensing [Karaduman *et al.* (2015), Hazra *et al.* (2015-a)], and solar cells [Zeng *et al.* (2011), Paul and Giri (2017)] applications. However, the fabrication of good quality n-TiO_2 thin films (TFs) on bulk p-Si substrates without using a buffer layer is challenging due to the mismatching in the values of lattice constants and thermal expansion coefficients of Si and TiO_2. Among various TiO_2 TF deposition techniques such as the Sputtering [Martin *et al.* (1996), Selman and Hassan (2015)], Electron-Beam Evaporation (EBE) [Vishwas *et al.* (2012)], Metal Organic Chemical Vapour Deposition (MOCVD) [Pradhan *et al*. (2003)], Atomic Layer Deposition (ALD) [Pore *et al.* (2004)], Sol-gel (SG) methods [Alam and Cameron (2002), Xie *et al.* (2011)], Pulsed Laser Deposition (PLD) [Mazhir *et al.* (2015)], Chemical Bath Deposition (CBD)) [Selman *et al.* (2014), Selman and Hassan (2015)], Spray Pyrolysis [Shinde *et al.* (2009)], Anodization [Yang *et al.* (2013)], and Hydrothermal [Zhang *et al.* (2015-a)] used for the deposition of TiO_2 TFs on a varieties of substrates including quartz [Vishwas, *et al.* (2012)], glass [Tsai *et al.* (2011)], Fluorine-doped tin oxide (FTO)-coated glass [Zhang *et al.* (2012-a)], ITO [Mechiakh *et al.* (2011)], Ti [Yang *et*

al. (2013)], and Silicon [Selman and Hassan (2015)], the SG and EBE methods are considered to be the simplest and low-cost deposition techniques for fabricating the low-cost p-Si/n-TiO_2 TF heterojunction devices. Si is the most preferred substrate due to its low-cost, easy availability, well-matured processing technology and possibility of integration of the Si based devices with the well-developed IC technology for enhancing their performance and functionalities as discussed in the previous chapter. In view of the above, present chapter deals with the fabrication, characterization, and UV detection properties of two types of bulk p-Si/n-TiO_2 TF heterojunction UV photodiodes obtained by depositing the n-TiO_2 TFs directly on the bulk p-Si <100> substrate using two different techniques: Sol-gel (SG) and E-Beam Evaporation (EBE). The layout of this chapter is given as follows:

Section 2.2 presents the experimental details of bulk-Si/TiO_2 heterojunction diode fabricated via SG and EBE methods. Section 2.3 briefly introduces various techniques used for the characterization of EBE and SG based TiO_2 TFs and p-Si/n-TiO_2 heterojunction diodes under study. Section 2.4 presents the results and discussions of the morphological, electrical and optical characteristics of the p-Si/n-TiO_2 TF heterojunction photodiodes. Finally, Section 2.5 is used to summarize important observations of this chapter.

2.2 Experimental Details

In the present section we will discuss the experimental details and procedure used for the fabrication and characterization of the Si/TiO_2 heterojunction diodes grown by two methods i.e. SG and EBE. The device fabrication includes substrate cleaning, TiO_2 TFs deposition, post annealing treatment, deposition of anode and cathode sequentially for ohmic contacts formation followed by post-fabrication annealing. Figure 2.1 illustrates

the layout of the fabrication steps in the form of a flowchart. This section has been divided into following subsections to discuss fabrication steps in details.

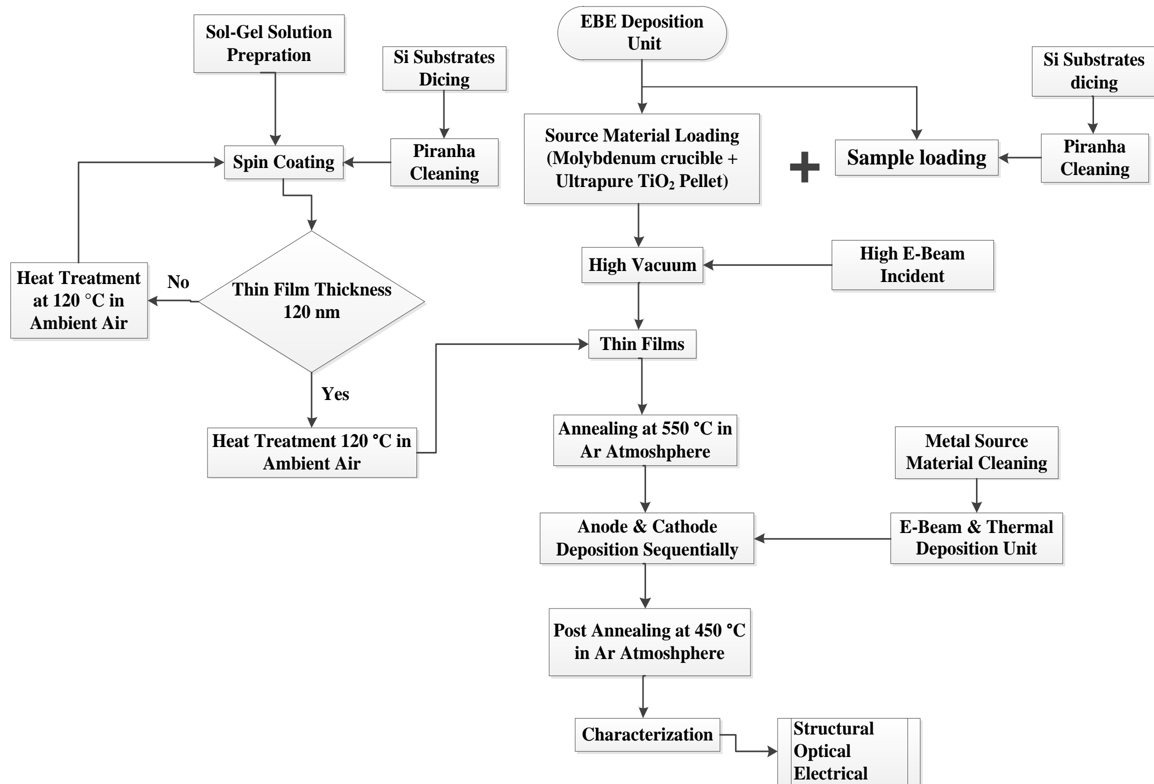

Figure 2.1: Flowchart of the experimental procedure.

2.2.1 Substrate Cleaning

In the present work, single side polished boron doped p-type <100> 4″ diameter Si wafers (Wacker-Chemitronic GmbH, Germany) with thickness ≈345-445 μm and resistivity ≈2−7 Ω.cm were cut into small regular stripes using diamond cutter. The small p-Si substrate pieces were then cleaned thoroughly. At first the p-Si substrates were cleaned ultrasonically in a sequence with trichloroethylene (TCE) and isopropyl alcohol for 10 min. each to remove certain metal contaminants and organic residues. Then, the Si substrates were subsequently immersed in a solution of H_2SO_4 and H_2O_2 (40:60 by volume) at 80 °C for 20 min. and then in a solution of hydrogen fluoride (HF)

and deionized (DI) water (1:10 by volume) for 1 min. After each step of cleaning procedure, the Si substrates were thoroughly quenched by DI water (multiple times) with resistivity (ρ) of ~18 MΩ.cm to get rid of chemical residues. We used the DI water from Millipore i.e. Model Milli-Q water plant of Millipore, USA. Finally, the samples were dried in a temperature controlled oven at 110 °C for 20 min. The H_2SO_4 (purity ~97 %) and H_2O_2 (purity ~30 %) solution dipping is used to remove the atomic, ionic and organic contamination from the substrates. The final rinsing in HF solution is done with a purpose to etch out the native silicon dioxide layer from surface of the substrates. The above mentioned procedure is well known as Piranha Cleaning method. All the chemicals used were purchased from MERK-Chemical Limited, Mumbai, India and were used without further purification. For transmittance characterization of the TiO_2 films, we have deposited the SG and EBE based TiO_2 films on a transparent substrate like glass. For this, the glass substrates were first thoroughly cleaned with the soap solution. Then glass substrates were rinsed and ultrasonically cleaned with trichloroethylene (TCE) and isopropyl alcohol for 10 min. each. Lastly rinsed with running DI water and then placed in a temperature controlled oven at 120 °C to dry the water content from substrate surface.

After cleaning, two batches of substrates were prepared for TiO_2 TF deposition via two independent techniques i.e. EBE and SG. We have used above mentioned procedure of p-Si wafer cleaning for fabricating various devices presented in Chapter-2 to Chapter-5 of the present thesis.

2.2.2 TiO_2 Thin Film Deposition by EBE Method

Immediately after cleaning the substrates as mentioned in Section 2.2.1, we have used ultra-high purity TiO_2 powder in the EBE unit for the deposition of TiO_2 TFs on the

polished surface of the cleaned Si wafers. The ultrapure TiO_2 powder (purity ~99.99 %) from MERK-Chemical Limited, Mumbai, India has been pressed to form pellets of 8 mm diameter to be used as the source material in the EBE deposition unit (HINDVAC, Bangalore, India; Model No. FL400, SMART COAT 3.0 A). To solidify the pellets and to decompose the Polyvinyl Alcohol (PVA) (used as a binder), the TiO_2 pellets were heated in the ambient air atmosphere at 1200 °C for 3 hours. Then the thoroughly cleaned and dried substrates were placed in the EBE chamber and the source material (TiO_2 pellets) was kept in the EBE unit under high vacuum (~10^{-6} mbar). Then the high energy electron beam was focused on to the TiO_2 pellets placed in molybdenum crucible to vaporize TiO_2 at high vacuum (~10^{-6} mbar) with a deposition rate of 1.00 Å/s inside the EBE deposition unit. The TiO_2 TF of thickness ~120 nm was deposited on the p-Si substrates placed at ~18 cm from the source in the EBE unit. The vacuum during the deposition in the deposition chamber was maintained in the range of ~10^{-5} to ~10^{-6} mbar. The rate of evaporation and thickness of the film were monitored using the in-built digital thickness monitor from INFICON with model no. SQM-160.

2.2.3 TiO_2 Thin Film Deposition by SG Method

2.2.3.1 Synthesis of Sol-gel Solution

For making a Sol-gel (SG) solution, we have used titanium tetraisopropoxide [$Ti(OC_3H_7)_4$, ex. Ti ≥ 98 % Merck] as a starting precursor due to its better solubility in alcohols as compared to the commonly used titanium n-butoxide [González *et al.* (2007), Alaie *et al.* (2015)]. The precursor of 12 cc was dissolved in 170 cc of isopropyl alcohol (C_3H_8O) to prepare the SG for TiO_2 TF deposition. The solution was then kept on a magnetic stirrer for 1 hour at room temperature. As a final step, a few drops of Hydrochloric acid [HCL, 2 M, 35 % Merck] were gradually added in the solution until a

transparent SG solution was obtained. The final solution was subjected to the magnetic stirrer for 3 hours at room temperature. In this process, the HCL was used as a catalyst to accelerate the process of hydrolysis [González *et al.* (2007)]. The SG coating was made after aging the solution for 24 hours and filtering it through the PVDF membrane of 0.22 μm pores size from MILLEX GV Filter unit. The SG solution filtering ensures that the larger size particles are filtered out from the solution. Further the molarity of as synthesized SG solution was ≈248.35 mMole. A simple flow chart to demonstrate the SG synthesis process is illustrated in Figure 2.2.

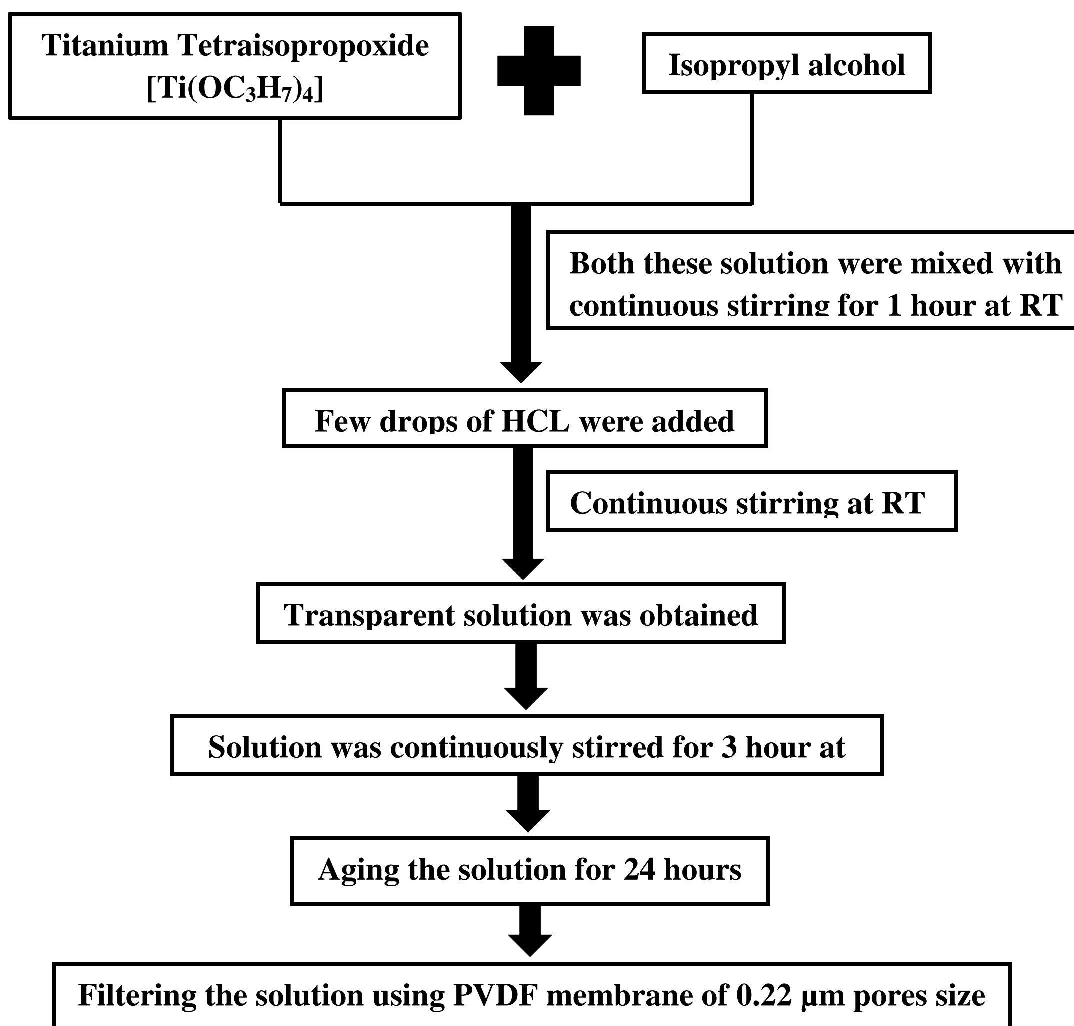

Figure 2.2: A simple flow chart to demonstrate the Sol-gel synthesis process.

2.2.3.2 TiO_2 Thin Film Preparation by Spin Coating Method

The Sol-gel was further used for spin coating to obtain the desired TiO_2 TF thickness (~120 nm). The spin coating unit (TSE, Model: SPM-150LC, Germany) was used for the TiO_2 TF deposition. With the help of a micro-dropper, the prepared SG solution was dropped onto the cleaned polished side of p-Si and glass substrates placed over the substrate holder of spin coater unit, which were then spin-coated at 3000 r/min (rpm) and 2000 r/min (rpm) for 30 sec., respectively. Then, the spin coated TiO_2 TFs were kept in a temperature controlled oven at pre-heated temperature of ~120 °C for 20 min. The process was optimized and finally repeated for three times (at same speed and duration) to achieve a final film thickness of ~120 nm sequentially followed by above mentioned heat treatment. The rotational speed was selected in order to have uniform spreading of the SG solution over selected substrate. The sequential heat treatment removes the organic materials and dries the TiO_2 TF surface. Further, the TiO_2 film thickness was measured by an optical spectrometer commonly known as F20-UV, thin film analyser (Model No. LSDT2, FILMETRICS). Now, for the TF characterization purpose, the samples were cooled down at room temperature and processed further as mentioned in the following sections.

2.2.4 Annealing of TiO_2 Thin Films

Rapid thermal annealing (RTA) or annealing is the process of heat treatment generally used to modify the semiconductor properties [Xu *et al.* (2002), Rollett *et al*. (2004)]. It involves heat treatment at a particular temperature for a certain period of time under a suitable gas environment. The materials can relieve internal stresses during annealing period to improve their properties by making them regular and soften with induced ductility [Rollett *et al*. (2004), Ranjitha *et al.* (2013)]. In view of the above, the SG and

EBE derived TiO_2 TF samples were processed for RTA under certain controlled environment. The samples were placed in the quartz annealing furnace (from Thermco, U.S.A) for post-deposition annealing at 550 °C for 20 min. in inert Argon (Ar) gas atmosphere with the gas flow rate of ~30 sccm into the furnace. This post-deposition annealing treatment of the TiO_2 TFs was used to improve the crystalline quality of the TiO_2 TFs by reducing the structural surface defects of the films [Vishwas *et al.* (2012)]. After the annealing, the samples were cooled down to the room temperature for further processing as discussed in the following sub-section. One batch of TiO_2 TF samples under consideration was processed for the film characterization purpose while the second batch of TiO_2 coated p-Si samples were processed for the fabrication of p-Si/n-TiO_2 heterojunction UV photodiodes under study.

2.2.5 Formation of Ohmic Contacts

In order to inspect the electrical characteristics of p-Si/TiO_2 heterojunctions (under consideration), the formation of ohmic anodes and cathodes is mandatory. For p-Si/n-TiO_2 based heterojunction device fabrication, the annealed TiO_2 TFs under consideration were placed in the vacuum deposition unit consisting of both the EBE and Thermal evaporation facilities (Model No. FL400, SMART COAT 3.0 A, Hind High Vacuum, India). The vacuum level was maintained in the range of ~10^{-5} to ~10^{-6} mbar while other conditions of the deposition were maintained to be same as used for the TiO_2 film deposition method discussed in Section 2.2.2. First, highly pure Titanium (Ti) (purity ~99.99 %) and Aluminium (Al) (purity ~99.99 %) were cleaned ultrasonically in a sequence with trichloroethylene (TCE) and isopropyl alcohol for 10 min. each. Cleaned Ti and Al metals were used as source materials for contact electrodes deposition. For formation of ohmic metal contact for cathode electrode, high purity

(99.99 %) Ti/Al (70 nm/50 nm) bilayer metallization in the form of circular metal dots of ~1 mm diameter (i.e. ~0.785×10^{-2} cm^{-2}) were sequentially deposited by the EBE method on both the EBE and SG derived TiO_2 TFs using the shadow mask technique. For the anode contact of p-Si/n-TiO_2 heterojunction photodiodes under study, the entire non-polished surface of the bulk p-Si substrates (i.e. at the opposite side of the TiO_2 film of the substrate) was uniformly metalized with Ti/Al (50 nm/40 nm) bilayer stacked metallization using EBE deposition method. It may be mentioned that EBE method was preferred over the thermal evaporation method due to its ability to provide good ohmic contacts of lower resistance than thermal evaporation method [Tsai *et al.* (2011), Somvanshi *et al.* (2014), Alaie *et al.* (2015)]. In the Ti/Al bilayer stacked structure for metal electrodes, we preferred using Ti metal layer under the Al layer due to its superiority for making stable ohmic contact with TiO_2 TFs [Ting and Wittmer (1982), Kim *et al.* (2002), Zalar *et al.* (2002)] through the formation of some intermediate phases like Al_3Ti [Kim *et al*. (2002)].

2.2.6 Post Fabrication Annealing

All the post-metal deposited samples were finally processed for the RTA at 450 °C for 7 min. in the Ar gas atmosphere with a flow rate of Ar ~30 sccm for improving quality of the metal electrodes [Somvanshi *et al.* (2014), Hazra *et al.* (2014-c), Karaduman *et al.* (2015)]. The post-fabrication annealing treatment mainly improves the quality (in terms of adhesion and stability) of the electrical contacts as suggested by other researchers [Brillson and Lu (2011), Kinaci and Ozcelik (2013), Karaduman *et al.* (2015)]. Figure 2.3 displays the schematic diagram for the complete fabrication procedure of p-Si/TiO_2 TF heterojunction diodes under consideration.

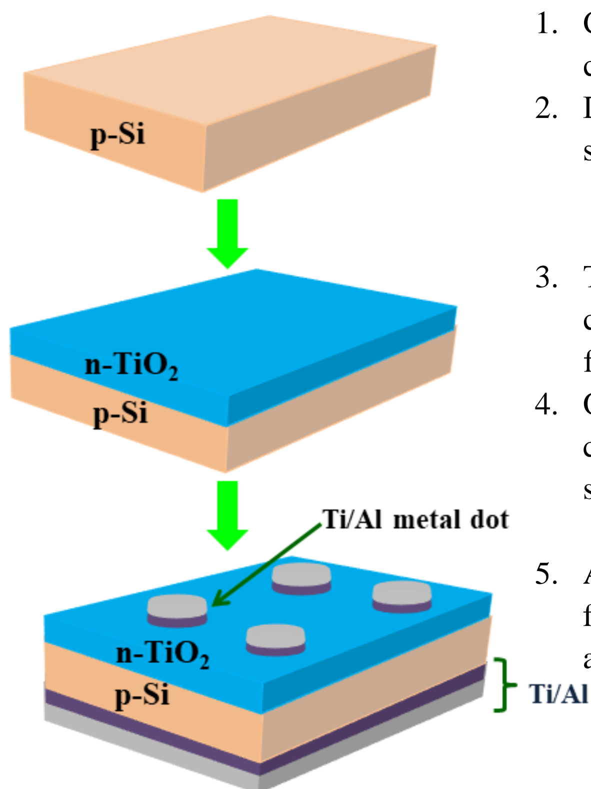

1. Cleaning of p-Si substrates by standard cleaning procedure
2. Deposition of TiO_2 TF (~120 nm) on p-Si substrates using two different methods:
   - ✓ *SG*
   - ✓ *EBE*
3. The annealing treatment of TiO_2 TFs is carried out in Ar gas atmosphere at 550 °C for 20 minutes.
4. On the top surface of TiO_2 TFs, Ti/Al contacts are fabricated by EBE method using shadow mask technique.
5. After electrical contacts deposition, the post fabrication annealing is carried out in Ar gas atmosphere at 450 °C for 7 minutes.

Figure 2.3: Schematic diagram of the fabrication steps used for the preparation of p-Si/n-TiO_2 TF heterojunction diodes.

2.3 Characterization Methods of p-Si/n-TiO_2 Heterojunctions

It is already discussed in Chapter-1 that properties of TiO_2 nanostructures depend on various parameters such as the deposition environment, film quality, deposition method, temperature, duration of annealing and substrates used for the film deposition. Thus in order to understand the deposition technique dependent properties of the SG and EBE derived TiO_2 TF on bulk p-Si <100> substrate, we will investigate its morphological, structural, electrical and optical properties by using various sophisticated analytical instruments. We have investigated the structural properties for surface morphology and crystallographic orientation by analysing High Resolution Scanning Electron Microscope (HRSEM), SEM, Atomic Force Microscopy (AFM), X-Ray Diffraction

(XRD) results. The room temperature optical properties of the TiO_2 films have been studied by analyzing the photoluminescence (PL), Reflectance, Transmittance, and UV-Vis spectroscopic results. The resistivity, electron concentration and mobility of the films have been investigated using the four probe and Hall measurements. The I-V and C-V characteristics of the two types of p-Si/n-TiO_2 heterojunctions containing the SG and EBE based films have been studied by the semiconductor parameter analyzer (Keysight, B1500A). The photodetection properties of the heterojunction photodiodes have been studied by using an UV source with output optical power rating of ~650 μW at ~365 nm wavelength [Benchmark, India]. The UV illumination was incident on the device to measure the UV-dependent I-V characteristics at room-temperature.

2.4 Results and Discussion

In the present section and its sub-sections some important discussions with reference to the details of analytical characterization results are presented. The basic measurement techniques are already discussed in the introduction section of Chapter-1. Thus in the following sections we have presented the discussion for the analysis of our measured results.

2.4.1 Characterization of As-Prepared Sol-gel Solution

2.4.1.1 Surface Morphology and Crystallographic Characterization

The as-prepared SG solution was first thoroughly washed in methanol and then dispersed in isopropyl alcohol and ultrasonicated for few minutes. Later the solution was drop casted over a copper (Cu) grid of the transmission electron microscopy (TEM) instrument (TECHNAI G2 20 TWIN JEOL 6400). The TEM analysis is used to investigate the crystalline phase, preferred orientation, dispersion properties and size of

nanocrystalline TiO_2 of the as-synthesized SG TiO_2 solution. Figure 2.4 shows the TEM image of the as-synthesized SG solution on Cu grid. The TiO_2 nanoparticles of sizes ranging from ~1.5 nm to 3 nm are found to be agglomerated which ensures a continuous and uniform deposition of TiO_2 TF on any substrate.

In order to study the crystallinity of the as-prepared TiO_2 solution, Selected Area Electron Diffraction (SAED) pattern was analyzed and is shown in Figure 2.5. The diffraction pattern shows the anatase crystalline structure (tetragonal crystal structure) of TiO_2 with lattice parameters of a =3.7850 Å and c =9.5196 Å which are matched with the Crystallography Open Database (COD), card number COD-7206075 [Rezaee *et al.* (2011)]. In Figure 2.5 we observed continuous diffused concentric rings in the SAED pattern for multiple particles on Cu TEM grid. The diffraction pattern or orientation of TiO_2 particles can be confirmed by the analysis of rings present in SAED pattern. The four rings are indexed to <024>, <015> <020> and <011> reflections of the anatase phase TiO_2 with a d-spacing of 1.4813 Å, 1.7009 Å, 1.8925 Å, and 3.5172 Å, respectively. The result of Figure 2.5 ensures the small particle size of TiO_2.

The associated Energy dispersive X-ray spectrometry (EDX) of the same sample is illustrated in Figure 2.6 with the peaks for Cu, Ti and oxygen element. The weight percentages of Cu, Ti and oxygen are ~55.08 %, 4.84 % and 40.08 %, respectively while their respective atomic percentages are ~24.96 %, 2.91 % and 72.13 %. The respective weight % and atomic % for each individual element present are also mentioned in the inset table of Figure 2.6. The weight % and atomic % indicate good chemical stoichiometry for TiO_2 formation. In addition EDAX spectra have the dominant peak of Cu which is attributed to the Cu TEM grid acting as a substrate. The absence of any additional material peak confirms the purity of our as-synthesized SG solution which is further used for the TF preparation by spin coating method.

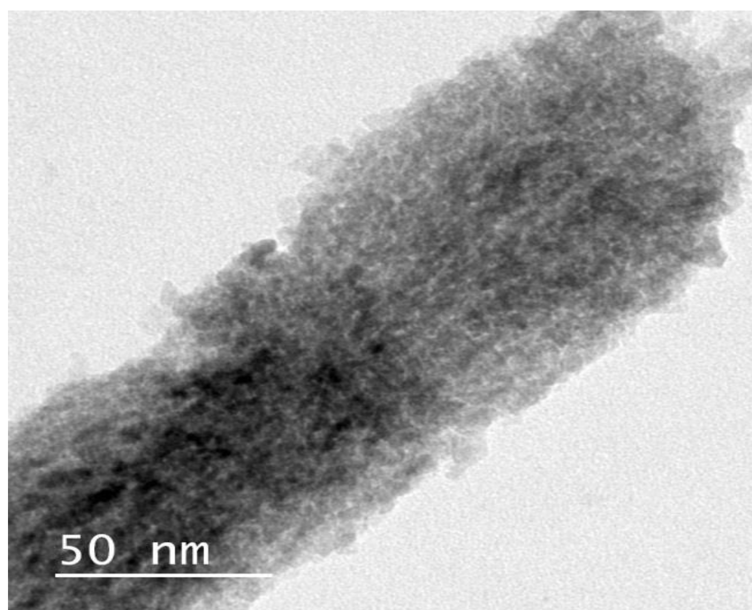

Figure 2.4: Transmission Electron Microscopy (TEM) image of as-grown TiO_2 anatase nanoparticles.

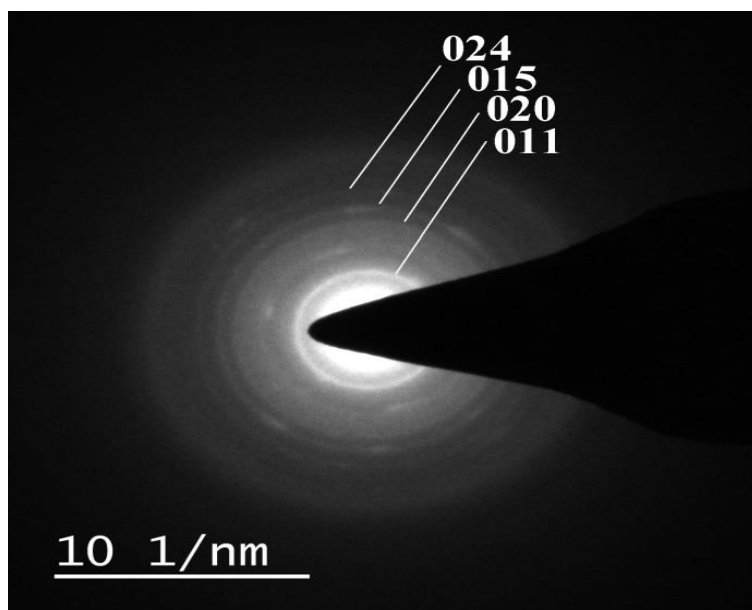

Figure 2.5: Selected Area Electron Diffraction (SAED) pattern of as-grown TiO_2 nanoparticles.

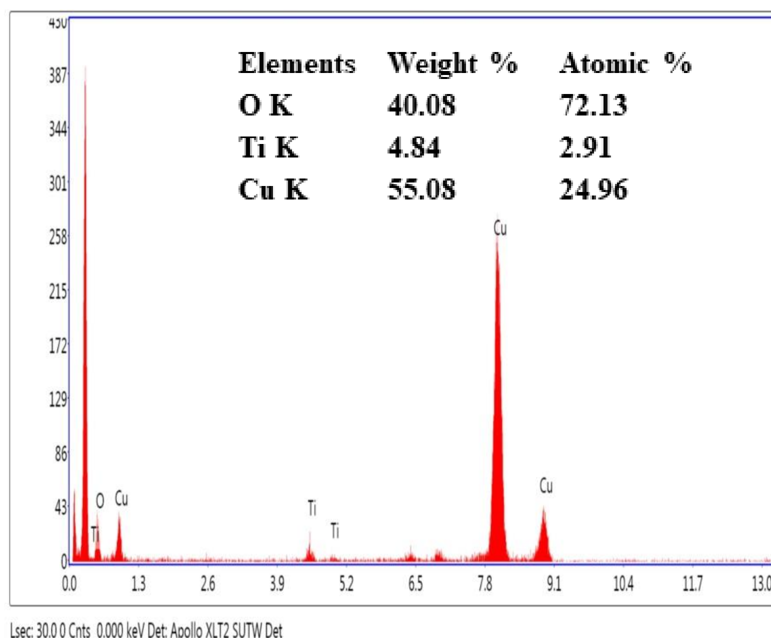

Figure 2.6: EDX/EDS spectra of as prepared TiO_2 nanoparticles on Cu TEM grid. Inset table illustrates the details of respective elements present.

2.4.2 Characterization of TiO_2 Thin Films

2.4.2.1 Surface Morphology Characterization

All the surface morphology characterization discussed in the following subsections have been investigated on bulk p-Si substrate.

(a) Surface morphology study by using AFM

The surface morphology of the TiO_2 TFs deposited on bulk p-Si substrates by EBE and SG methods has been analyzed by the Scanning Probe Microscopy (SPM) (Model No. NTEGRA Prima, NT-MDT Services and Logistics Ltd., Ireland) and shown in Figure 2.7 (a), (b), (c) and (d). Figure 2.7 (a) and (b) illustrates the 2D and 3D AFM image of the n-TiO_2 TF deposited using EBE method whereas Figure 2.7 (c) and (d) illustrates the 2D and 3D AFM image for the SG method. It is confirmed from the AFM images in Figure 2.7 (a), (b), (c) and (d) that the TiO_2 TFs deposited by both the methods are

nanocrystalline in nature. The surface roughness, root mean square (rms) roughness, grain size and grain length measured for the two types of films using Nova PX (AFM software) have been compared in Table 2.1.

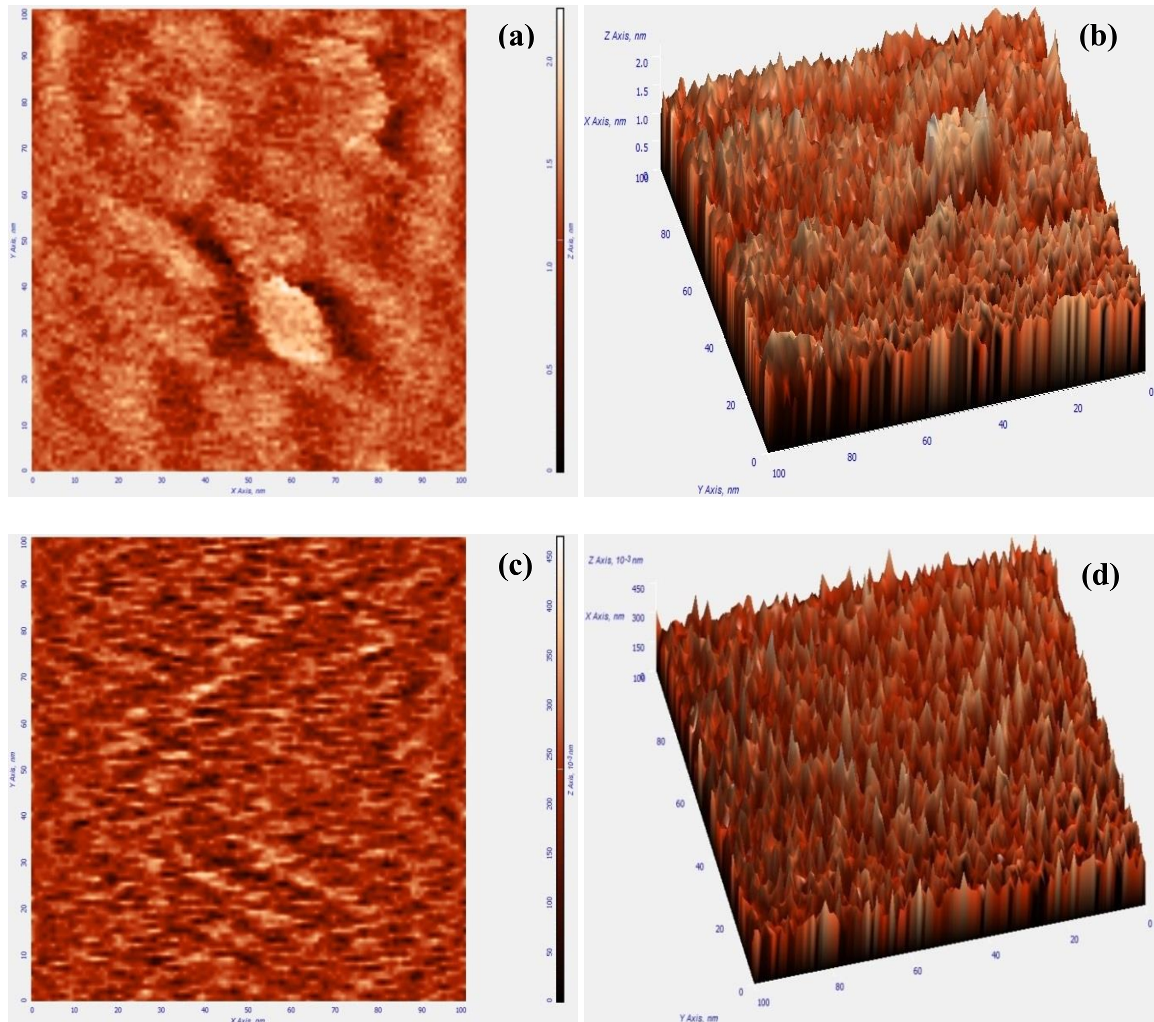

Figure 2.7: (a) 2D (b) 3D AFM image of the n-TiO_2 TF on p-Si substrate deposited using EBE method; (c) 2D (d) 3D AFM image of the n-TiO_2 TF on p-Si substrate deposited using SG method.

From the Table 2.1, the peak-to-peak spacing, root mean square, roughness average, average grains size and grains length are observed to be smaller for the SG based TiO_2 films than their respective values of the films deposited by the EBE method. The rms values of both types of films shown in the Table 2.1 are slightly smaller than those

reported by Touam *et al.* [Touam *et al.* (2013)] and Mechiakh *et al.* [Mechiakh *et al.* (2011)].

Table 2.1: Comparison of AFM Derived Parameters.

Parameters	**EBE**	**Sol-gel**
Sampling area (nm×nm)	250000.0	250000.0
Peak-to-peak spacing (nm)	7.781	0.436
Root mean square (nm)	0.483	0.0589
Roughness average (nm)	0.367	0.0467
Average grains size (nm)	14.152	12.848
Grains length (nm)	21.210	19.789

(b) Surface morphology study by using SEM and HRSEM

The Scanning Electron Microscopy (SEM) (EVO MA15/18, from Carl Zeiss Microscopy Ltd., UK) has been used to analyze the surface morphology shown in Figure 2.8 (a) and (b). The SEM images clearly show that the deposited TiO_2 TFs are homogeneous, uniform and cracks free. The high quality SG based TiO_2 films may be attributed to the filtration of large particles from the SG solution before processing to the spin-coater for deposition. However, we could not see any nanostructure in the SEM images possibly due to the poor resolution of the normal SEM instrument. To investigate further, we have also used HRSEM measurements for studying the surface properties of the TiO_2 TFs under investigation as shown in Figure 2.9. The HRSEM images of Figure 2.9 (a) and (b) clearly show the existence of nano-level surface roughness on the TiO_2 TFs prepared by the EBE and SG with spin coating methods. Further, the SG derived TiO_2 films have smaller particle size as compared to that of the EBE derived films. Thus, SG derived TiO_2 films are expected to have larger surface-to-volume ratio than the EBE based films. In other words, the SG based p-Si/n-TiO_2 heterojunction is expected to provide better electrical and photodetection properties than

the device fabricated using EBE derived TiO_2 TFs. Both the EBE and SG based TFs are found to be uniform, crack free and homogeneous as also observed from the SEM images shown in Figure 2.8 (a) and (b).

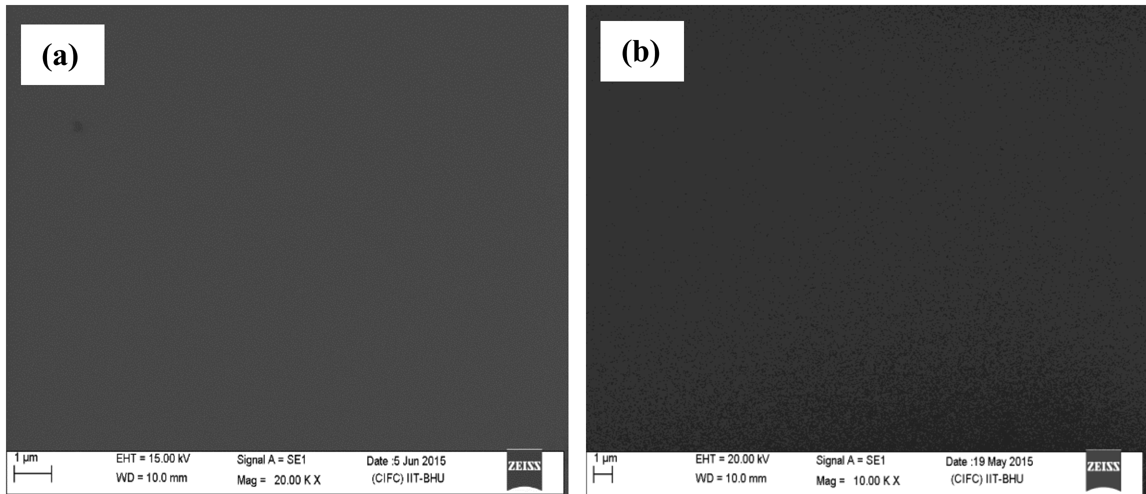

Figure 2.8: SEM images of n-TiO_2 TFs grown via (a) EBE method, and (b) SG method.

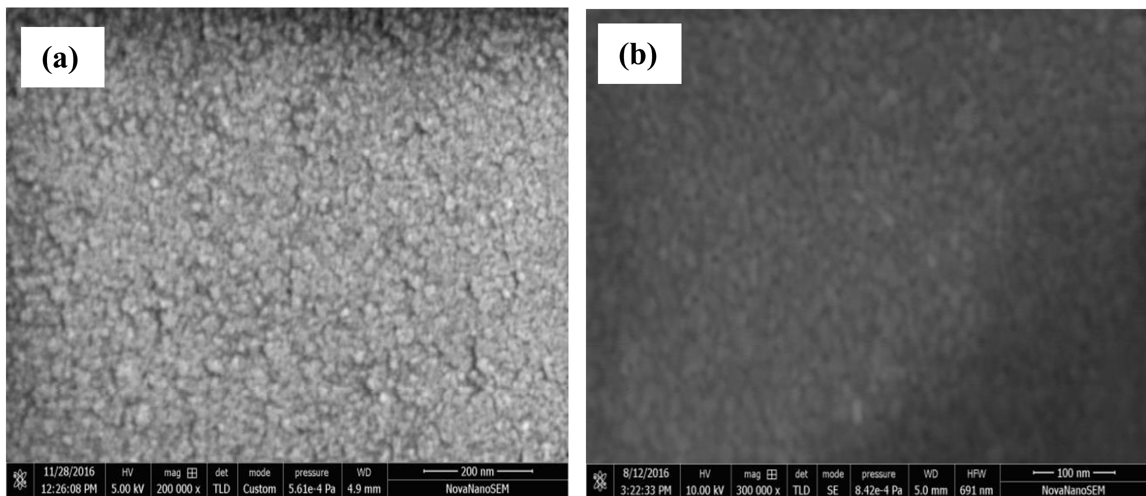

Figure 2.9: HRSEM images of n-TiO_2 TFs deposited via (a) EBE method, and (b) SG method.

(c) Crystallographic Orientation by XRD analysis

The crystalline structure of the EBE and SG based TiO_2 TFs have been investigated by the XRD (RIGAKU-Smart XDMAX, PC-20, 18-kW Cu rotating anode, Rigaku, Tokyo) data as shown in Figure 2.10 (a) and (b), respectively. The XRD spectrums were recorded for the TiO_2 TFs on p-Si substrate after RTA (as mentioned in Section 2.2.4). The figures clearly show the presence of both the anatase (JCPDS 89-4921) and brookite (JCPDS 00-002-0514) phases of TiO_2 in both types of films under study. In Figure 2.10 (a), the indexed diffraction peaks at $2\theta \approx 25.31^{\circ}$, 37.80˚, 51.96˚, 53.89˚ and 62.69˚ correspond to the reflections from the respective crystal planes (101), (004), (202), (105) and (204) of the anatase phase of TiO_2 [Thanigainathan *et al.* (2012)], the additional peak at ≈48.38˚ corresponds to (321) crystal plane of the brookite phase of the EBE derived TiO_2 TF [Grover *et al.* (2014)].

Similarly, the indexed peaks at $2\theta \approx 25.31^{\circ}$, 37.80˚, 53.89˚, 55.06˚ and 62.69˚ in Figure 2.10 (b) correspond to the reflections from the respective crystal planes (101), (004), (105), (211), and (204) of the anatase phase [Thanigainathan *et al.* (2012)] of the SG derived TiO_2 films whereas the peaks at 44.37˚ and 48.38˚ correspond to (221) and (321) crystal planes of brookite phase [Grover *et al.* (2014)], respectively. The anatase phase of TiO_2 is considered to be more photoactive than the rutile phase because of its larger specific surface area and easy hydroxylation [Jung *et al.* (2008)]. Anatase or rutile phases are typically the major product of inorganic syntheses of TiO_2. The anatase form is known typically as an n-type semiconductor [Karaduman *et al.* (2015)]. From XRD analysis, it is observed that the derived TiO_2 TFs via both the deposition methods are dominated by anatase phase. Further multiple diffraction peaks observed in Figure 2.10 (a) and (b) signify the polycrystalline nature of as deposited TFs.

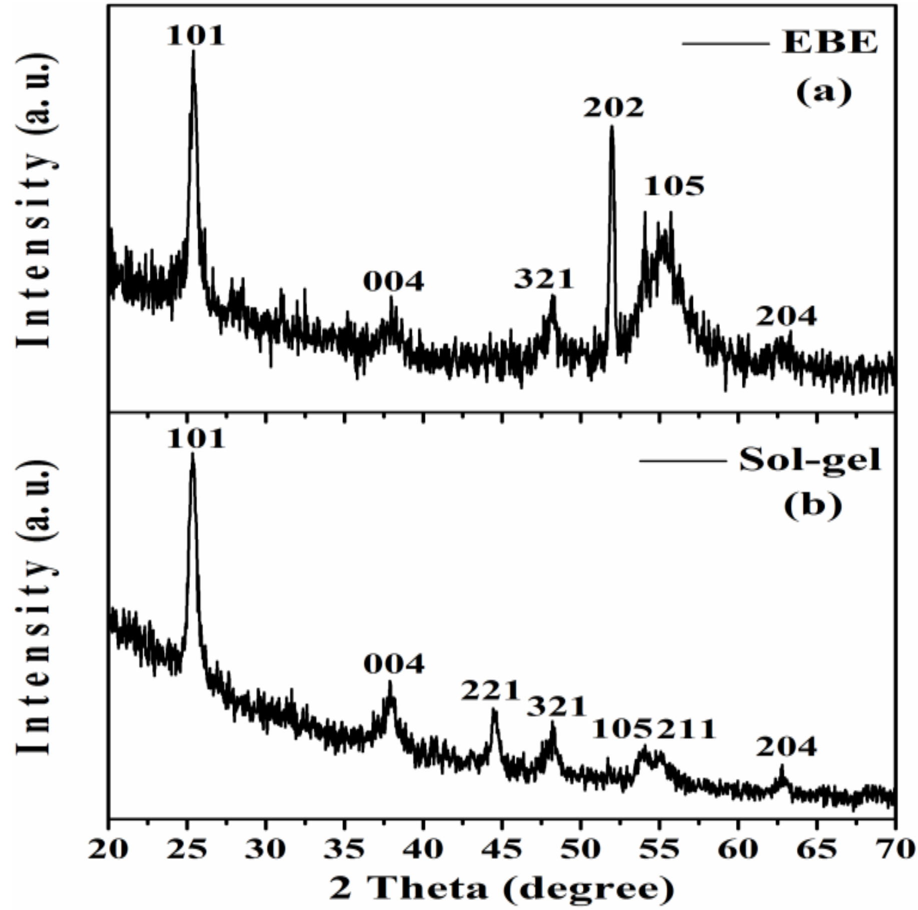

Figure 2.10: Typical XRD pattern of n-TiO_2 TFs on p-Si substrate for: (a) EBE method, (b) SG method.

The crystalline size of EBE and SG deposited TiO_2 TFs have been calculated by Debye-Sheerer formula given as:

$$D = \frac{k\lambda}{\beta \cos\theta} \tag{2.1}$$

where, k is a dimensionless shape factor with a typical value of about ~0.9, θ is the Bragg angle and β is the full width at half maximum (FWHM). Equation (2.1), thus, gives the values of crystalline size of the EBE and SG derived films as ~15 nm and ~12 nm, respectively. The smaller crystalline size in the SG derived TiO_2 TF than that of the EBE derived TF is in coherence with the AFM results discussed earlier. The smaller crystalline size implies larger surface-to-volume ratio of SG derived TiO_2 TF than that

of the EBE based film. Thus, it is expected that the SG based TiO_2 TF are more suitable for the sensing and detection applications than the EBE based films.

(d) Energy dispersive X-ray analysis

The chemical composition or elemental analysis of the TiO_2 TFs grown on p-Si substrates have been determined by Energy dispersive X-ray spectroscopy or analysis (EDS or EDAX) measurements and is shown in Figure 2.11 (a) and (b). The ratio of average weight % of Ti:O is 3.34:13.39 for EBE derived sample, whereas in case of SG derived sample its values are in the ratio of 5.49:14.02, respectively. The respective weight % and atomic % for each individual element present is mentioned in the inset table of Figure 2.11 (a) and (b). The decent ratio of weight % and atomic % demonstrates good chemical stoichiometry for the as grown TiO_2 TFs. In addition EDAX spectra shows the dominant peak of Si which is attributed to the bulk Si substrate. Further no peak of any additional material clearly illustrates that no impurities are present in the as grown TiO_2 TFs.

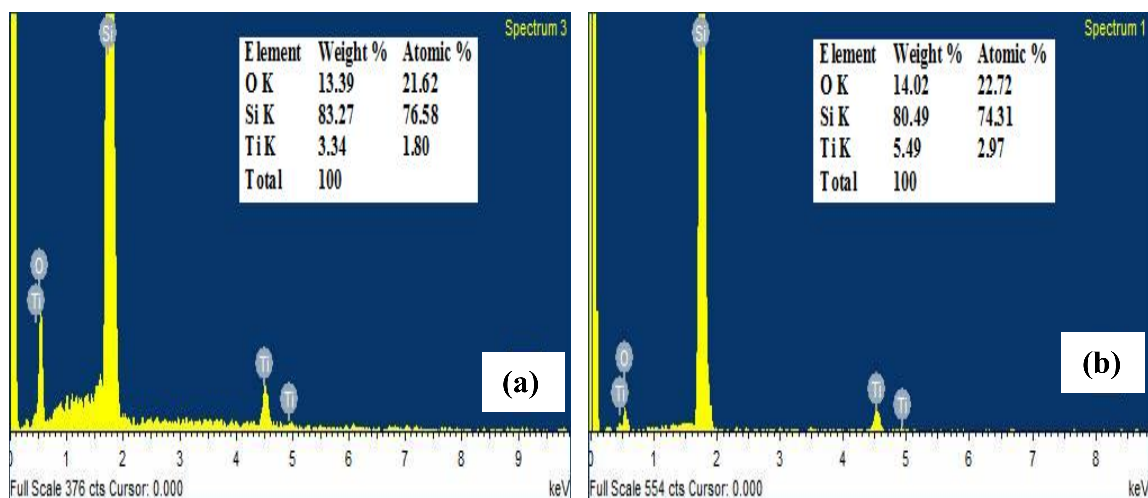

Figure 2.11: EDS spectra of as grown n-TiO_2 TFs on p-Si substrate for: (a) EBE method, (b) SG method. Inset table illustrates the details of respective elements present.

2.4.2.2 Optical Characterizations

Some brief discussion regarding optical measurement techniques are already presented in the introduction section of Chapter-1. Thus in the following sections we have presented the discussion for the analysis of our measurement results.

(a) Reflectance and Transmittance Measurement

Reflectance and transmittance measurements for the as grown TiO_2 TFs, have been carried out at room temperature using F20-UV, thin film analyzer (Model No. LSDT2) equipped with Filmetrics light source. For these optical measurements we have deposited the TiO_2 TFs on glass substrate via EBE and SG methods. Both reflectance and transmittance spectra were measured over the wide wavelength ranging from 200 nm to 1100 nm. For the following four figures (see Figure 2.12 and Figure 2.13) we have illustrated and compared the experimentally and theoretically estimated optical spectra for the as grown TiO_2 TFs (thickness ~120 nm), on a glass substrate after thermal treatments. For each figure we have mentioned "*Goodness of Fit*" (G.O.F) which signifies the accuracy of our experimental result (such as thickness) based on the fitting between theoretical and experimental plots. The theoretical reflectance and transmittance spectrum is calculated by Filmetrics thin film UV analyzer, based on the calculations of Fast Fourier Transform (FFT) and Discrete Fourier transform (DFT) algorithms. For theoretical calculations material characteristics such as extinction coefficient (k), thickness of TF, and refractive index (n) are used. Additionally, the indirect results such as absorption and band-gap can simply be estimated using direct results (reflectance and transmittance plots). For example absorbance = 100 – R – T (%), where, R is reflectance and T is transmittance [Du *et al.* (2015)].

Now first, we shall discuss the reflectance and transmittance spectra (see Figure 2.12 (a) and (b)) for sample prepared using the EBE technique. For Figure 2.12 (a) and (b) the associated G.O.F is ~87.62 % and ~97.73 % with reference to reflectance and transmittance plots which verifies the accuracy of our measured thickness ~120 nm. It is also observed that in the UV region reflectance peak has reached up to ~50 % and ~58 % for theoretically calculated and experimentally measured data, respectively. Whereas in case of transmittance plot for the same sample (see Figure 2.12 (b)), peak transmittance has reached up to ~80 % after ~400 nm wavelength. Further, we will investigate the reflectance and transmittance plots (see Figure 2.13 (a) and (b)) for second sample prepared using the SG method. For Figure 2.13 (a) and (b) the associated G.O.F is 93.45 % and 99.79 % with reference to reflectance and transmittance plots confirming the accuracy of our measured TF thickness. In addition the UV region reflectance has reached up to ~40 % and 50 %, and transmittance spectra after ~400 nm wavelength have reached up to ~65 and 75 % for the respective theoretically calculated and experimentally measured data (see Figure 2.13 (a) and (b)). For all the four figures (see Figure 2.12 and Figure 2.13) high values of G.O.F also indicate that our as grown TiO_2 TFs have uniform thicknesses, smoothness, and homogeneous layer.

Irrespective of the TF deposition method used we observed that the as grown TiO_2 TFs have higher reflectance and low transmittance below ~400 nm wavelengths which is attributed to the strong absorption of TiO_2 material. The increase of transmission intensity in the visible and near infrared light range exemplified that our deposited TiO_2 TFs are highly transparent over the wavelength range ~400 nm–1100 nm. Our results are supported by and in consistency with the other reported TF optical investigations which were given post annealing treatments [Taherniya and Raoufi (2016)].

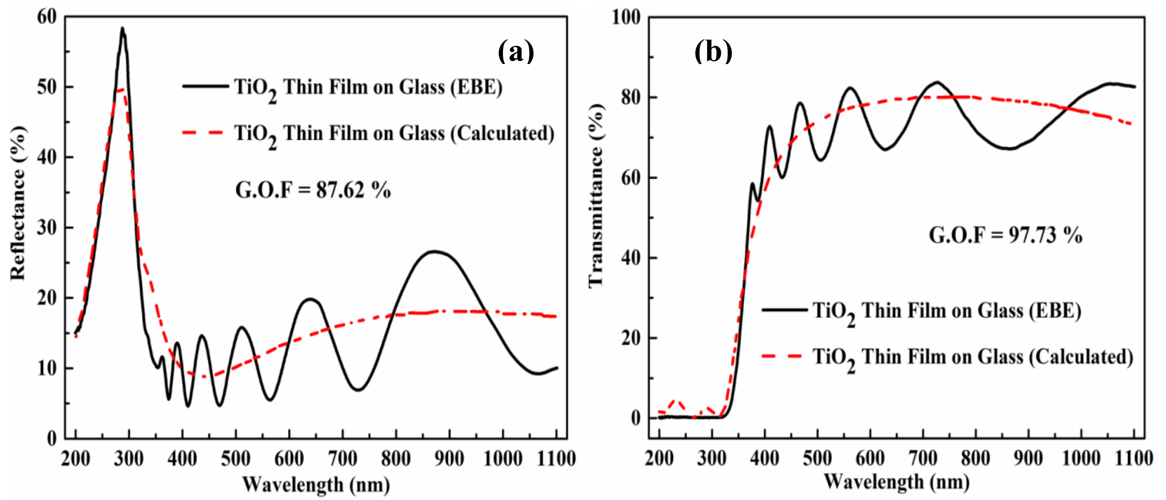

Figure 2.12: For EBE derived TiO_2 TF, comparative experimental and theoretical estimated plots of (a) Reflectance spectra, (b) Transmittance spectra.

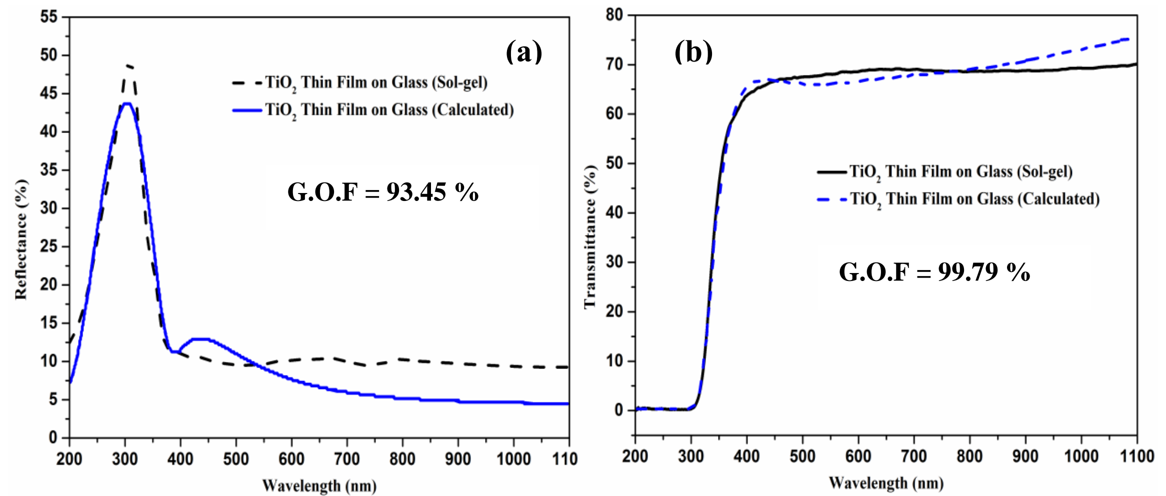

Figure 2.13: For SG derived TiO_2 TF, comparative experimental and theoretical estimated plots of (a) Reflectance spectra, (b) Transmittance spectra.

(b) UV-Vis Measurements

Ultraviolet–Visible (UV-Vis) spectrophotometry talks about absorption or reflectance spectroscopy which is typically used for the estimation of semiconductor band gap. To determine the band gap $\left(E_g\right)$ of TiO_2 TFs $\left(\text{of thickness } (d) \approx 120\,\text{nm, on glass}\right)$ under consideration, we have plotted $\left(\alpha(\lambda)\,h\nu\right)^2$ versus photon energy $\left(h\upsilon\right)$ curves as shown

in Figure 2.15. According to Beer-Lambert's law, the absorption coefficient $(\alpha(\lambda))$ of TF is given by the following relation [Ghobadi (2013)]:

$$\alpha(\lambda) = 2.303 \times \frac{Abs(\lambda)}{d} \tag{2.2}$$

where, d is TiO_2 TF thickness and $Abs(\lambda)$ TF absorbance. The absorption coefficient $\{\alpha(\lambda)\}$ is calculated from the absorbance spectra $\{Abs(\lambda)\}$, experimentally measured using UV-Vis spectrophotometer by Perkin Elmer Lambda-25. At room temperature the measured $Abs(\lambda)$ of the two TiO_2 TFs deposited via EBE and SG methods on glass substrates are displayed in Figure 2.14. For the two TiO_2 TFs under consideration we obtained the maximum absorption for UV region at a peak corresponding to ~307 nm wavelength. The absorption peak can be attributed to the charge transfer in absorption process involving an electron transfer [Nilchi *et al.* (2011)]. It is noted that the absorption in visible spectrum region is very small compared to the UV region, which suggests that as grown TiO_2 TFs have promising potential in the photodetector application for UV region [Wang *et al.* (2010-a)].

Further the absorption coefficient as a function of photon energy is expressed as: $(\alpha(\lambda)\, h\nu)^2 \propto (h\nu - E_g)$ [Sze (1981), Ghobadi (2013)], hence by extrapolating the linear part of $(\alpha(\lambda)\, h\nu)^2$ curve to $h\upsilon$ axis, where $(\alpha(\lambda)\, h\nu)^2 = 0$ (as demonstrated in Figure 2.15), the band gap energies of EBE and SG based TFs are estimated as ~3.1 eV and ~3.3 eV, respectively. Our estimated experimental values of the band gap are close to the reported band gap of anatase phase TiO_2 [Chinnamuthu *et al.* (2012)].

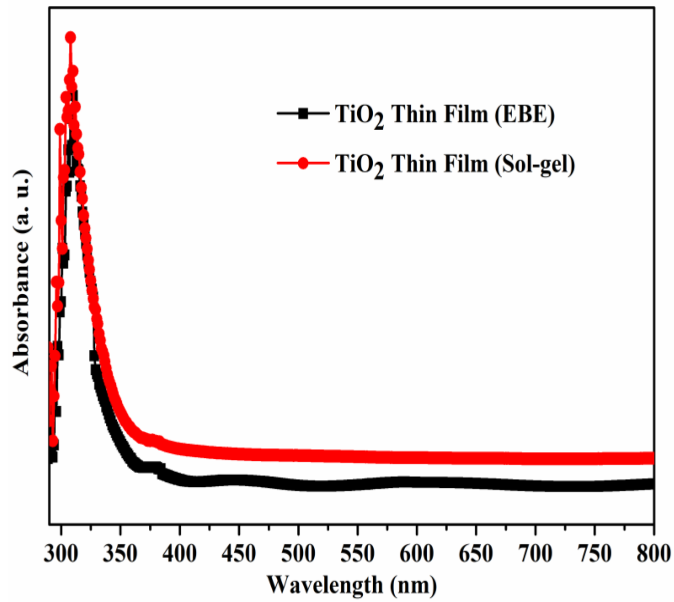

Figure 2.14: UV-Vis absorption spectra for EBE and SG deposited n-TiO_2 TFs on glass substrate.

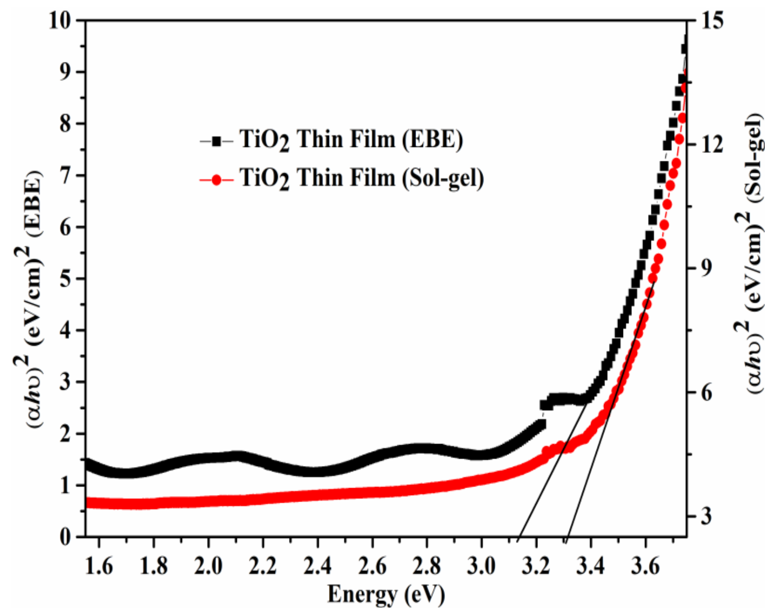

Figure 2.15: $(\alpha h\upsilon)^2$ vs. Energy $(h\upsilon)$ spectra for EBE and SG deposited n-TiO_2 TFs on glass substrate.

(c) Photoluminescence Measurements

To further characterize the optical properties of as grown EBE and SG derived TFs on p-Si substrate, detailed PL investigations were carried out with excitation wavelengths of ~250 nm (see Figure 2.16). Room temperature emission spectra as shown in Figure

2.16 and Figure 2.17, were measured using the instrument from Horiba with Model No: FL321. In Figure 2.16 although both the films show the strong emissions in UV region and weak emissions in visible regions, but the SG derived TiO_2 TFs are observed to have better emission spectra in the UV region. The strong peak at ~413 nm (i.e. ~3 eV) (see Figure 2.16) for both EBE and SG based samples is attributed to near band edge emission of TiO_2 TFs [Liu *et al.* (2005), Chinnamuthu *et al.* (2012)]. The other different peaks observed in PL spectra may be due to emissions from the surface states, oxygen vacancy and bulk defects [Liu *et al.* (2005)] since the oxygen vacancy and defects can act as level traps and cause luminescence. The main peaks in UV region observed in the PL spectra are very close to the direct band gap calculated from the UV-Vis measurements discussed earlier. Commonly, TiO_2 becomes n-type semiconductor due to the presence of defects such as oxygen vacancies and titanium interstitials [Vishwas *et al.* (2012)].

Now to justify the excitation wavelength of ~250 nm as used in Figure 2.16, we have considered EBE derived sample and excited it with three different wavelengths i.e. 250 nm, 270 nm and 325 nm (Figure 2.17). We observed that when excited wavelengths are changed, the PL intensity for emission plot is changed, but the fluorescent peaks are not shifted. This PL behaviour is in accordance with the theories considered for PL investigations [Gfroerer (2000), Liu *et al.* (2005)].

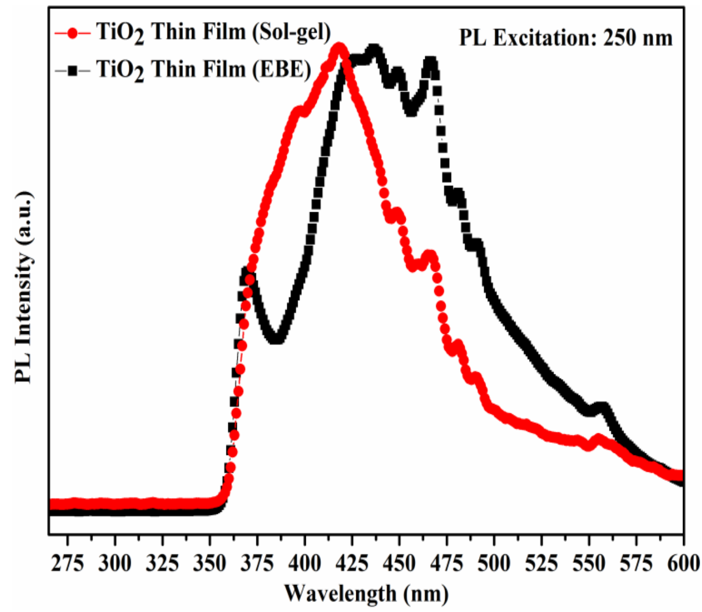

Figure 2.16: Room temperature PL Emission Spectra for the as deposited EBE and SG derived n-TiO_2 TFs. The excitation wavelength considered for this measurement is 250 nm.

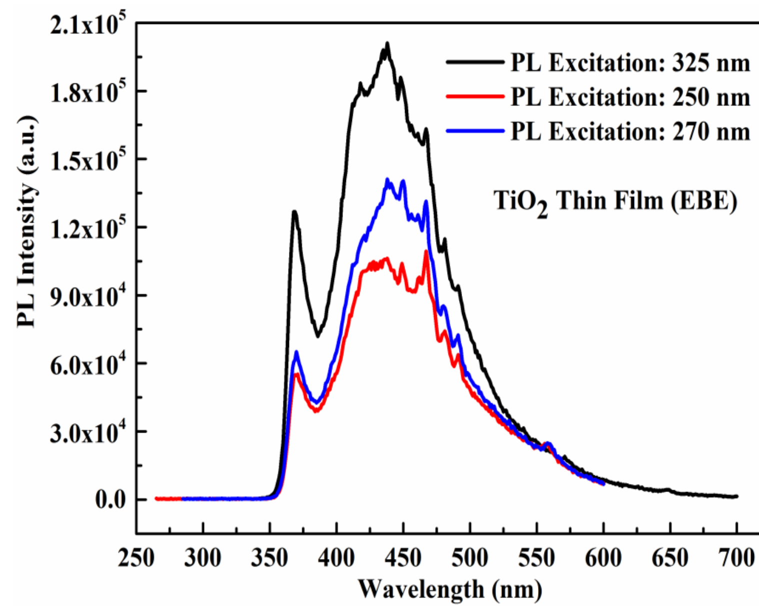

Figure 2.17: Room temperature PL Emission Spectra for EBE derived n-TiO_2 TF at different excitation wavelengths.

2.4.3 Electronic Properties

In the present section we have discussed and estimated some electronic parameters for the as-prepared TiO_2 TFs on p-Si substrates. By implying following relationships [Sze (1981)] on the four-probe technique and hall measurement data we examined various parameters. Basic Hall Effect measurement setup for n-TiO_2 TFs is also shown in Figure 2.18.

(a) Electrical Resistivity (ρ):

$$\rho = R_{sh} \times t, \text{ and } R_{sh} = \frac{\pi}{\ln(2)} \times \frac{\mathrm{V}}{\mathrm{I}} \tag{2.3}$$

where, R_{sh} represents sheet resistance, t is the thickness of TiO_2 TF, V is voltage drop across the inner probes and I is current across the outer probes.

(b) Donor concentration (N_D):

$$N_D = \frac{I \times B}{\mathrm{q} \times \mathrm{s} \times \mathrm{V_H}} \tag{2.4}$$

(c) Mobility (μ):

$$\mu = \frac{1}{\rho \times q \times N_D} \tag{2.5}$$

where, s represents distance between poles pieces (constant), B is magnetic field, V_H is Hall voltage, and σ is Conductivity.

The electronic properties of as-deposited TiO_2 TFs under consideration have been determined by Hall measurement (using magnetic flux density ~0.5 T) and four-probe technique with Advanced Instrument Technology (AIT) instrument having Model No. CMT-SR2000N). The electronic parameters such as donor concentration (N_D), resistivity (ρ), conductivity (σ) and mobility (μ) of the as-deposited TiO_2 TFs under consideration are listed in Table 2.2. The n-type natures of as-deposited TiO_2 TFs are ensured by the negative values of hall voltage [Sze (1981)]. It is observed that the

mobility and conductivity for the SG derived TF are higher than the corresponding values of the EBE deposited TF. Note that the carrier concentrations are within the range of ~10^{17} cm^{-3} to ~10^{20} cm^{-3} and hence are in good agreement with the results reported by Hwang *et al.* [Hwang *et al.* (2009)].

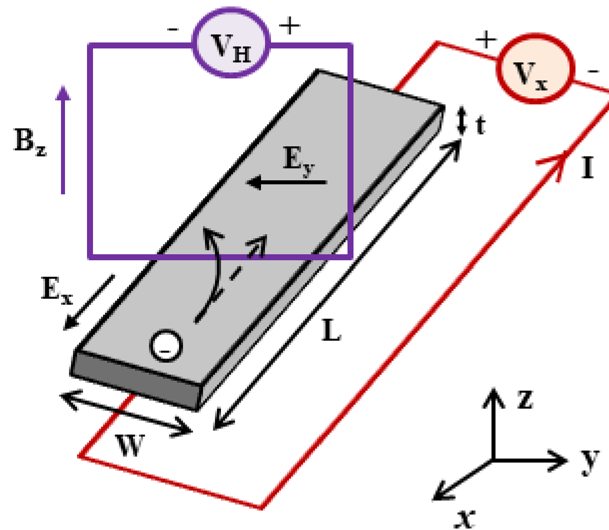

Figure 2.18: Hall effect measurement setup for n-TiO_2 TFs.

Table 2.2: Comparison of electronic parameters for TiO_2 TFs under consideration.

Method	N_D ($/cm^3$)	μ (cm^2/Vs)	ρ (mΩ.cm)	σ $(mΩ.cm)^{-1}$
EBE	3.25×10^{19}	83.48	2.3	0.434
Sol-Gel	1.59×10^{19}	184.96	2.13	0.469

2.4.4 Electrical Characterization of p-Si/n-TiO_2 Heterojunction Diodes

After investigating the TF properties, we will now examine the room temperature electrical characteristics via C-V and I-V measurements for the device structure as shown in Figure 2.19.

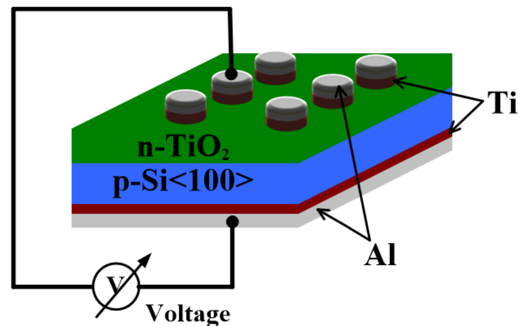

Figure 2.19: Schematic diagram of bulk p-Si/n-TiO_2 heterojunction diode.

(a) Characterization of Ti/Al Ohmic Contacts on n-TiO_2 TF and p-Si Substrate

To justify the suitability of the Ti/Al based ohmic contacts on the n-TiO_2 TFs and p-Si substrate for the cathode and anode electrodes of the p-Si/n-TiO_2 heterojunction under study, we have prepared two device structures shown in the inset of Figure 2.20 and Figure 2.21, respectively. For the structure in Figure 2.20, EBE based TiO_2 TF has been deposited on the SiO_2 (~300 nm thickness) obtained by the dry-wet-dry sequential oxidation of the cleaned p-Si substrate for 15 minutes each at 1100 °C. The EBE based TiO_2 film is then annealed at 550 °C for 20 minutes as discussed in earlier section. On the annealed n-TiO_2 TFs of Figure 2.20, Ti (~70 nm) and Al (~50 nm) metal dots of 1 mm diameter have been sequentially deposited by shadow masking technique as discussed earlier. Similarly, Ti (~50 nm) and Al (~40 nm) metal dots of 1 mm diameter have also been deposited for obtaining the ohmic contacts on the p-Si substrate of the structure shown in Figure 2.21. Both the Al/Ti/n-TiO_2/Ti/Al and Al/Ti/p-Si/Ti/Al

structures are then annealed at 450 ºC for 7 minutes in Ar gas environment for improving the quality of the ohmic contacts as discussed earlier.

The measured I-V characteristics of the Al/Ti/n-TiO_2/Ti/Al and Al/Ti/p-Si/Ti/Al structures have been shown in Figure 2.20 and Figure 2.21, respectively. The nearly linear I-V characteristics of both the Al/Ti/n-TiO_2/Ti/Al and Al/Ti/p-Si/Ti/Al structures confirm the formation of reasonably good Ti/Al based ohmic contacts on both the EBE based TiO_2 film and p-Si substrates. The ohmic characteristics of Ti electrode over TiO_2 and Si have also been reported by others [Chang *et al.* (2010), Hossein-Babaei and Rahbarpour (2011), Motayed *et al.* (2011), Pillai *et al.* (2014), Hazra *et al.* (2015-b), Jahromi *et al.* (2016)]. It may be mentioned that similar ohmic characteristics can also be achieved for the SG based TiO_2 films. Thus, Ti/Al metal contacts used for making the cathode and anode electrodes of the p-Si/n-TiO_2 heterojunction diode under investigation are well justified.

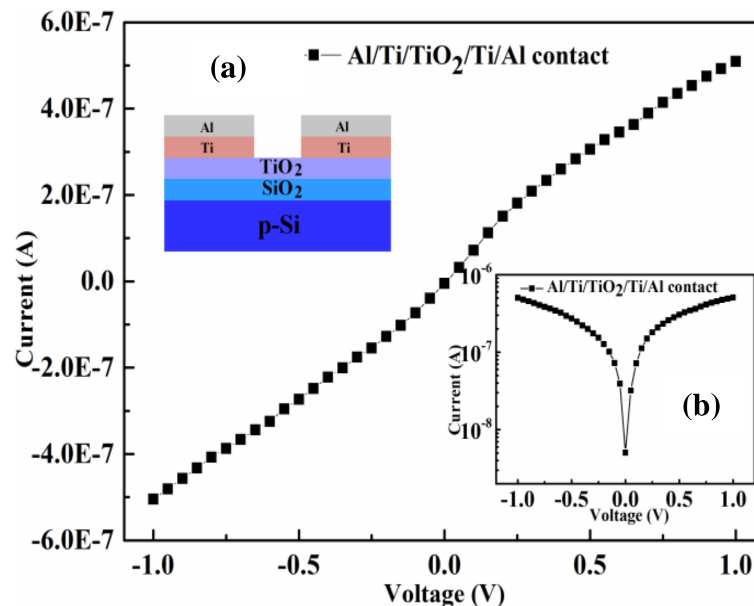

Figure 2.20: Electrical I-V characteristics for ohmic contact formation on TiO_2 TF. Inset figure (a) illustrates the schematic diagram of its respective device structure and (b) demonstrates its semi-log I-V plot.

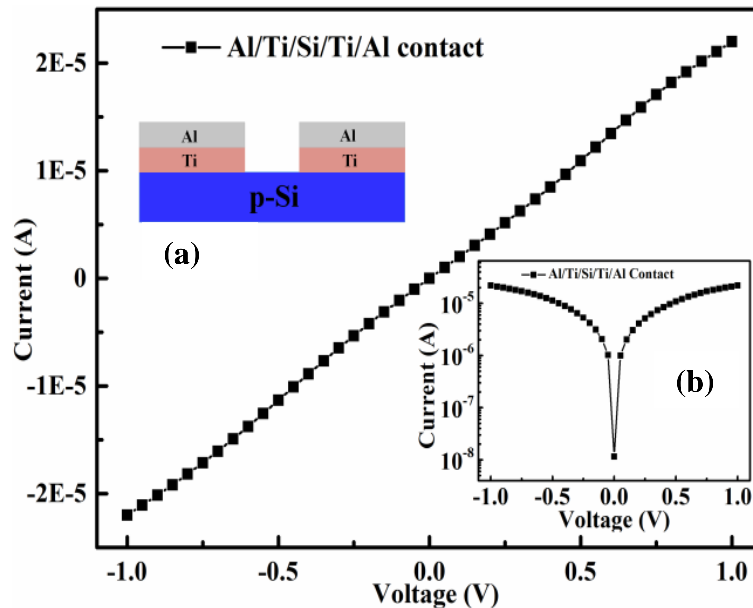

Figure 2.21: Electrical I-V characteristics for ohmic contact formation on non-polished side of Si substrate. Inset figure (a) illustrates the schematic diagram of its respective device structure and (b) demonstrates its semi-log I-V plot.

(b) Capacitance-Voltage Characteristics

Figure 2.22 and Figure 2.23 illustrate the room temperature (T ~303 K) Capacitance–Voltage (C-V) characteristics measured at high frequency of 1 MHz using semiconductor parameter analyzer (Keysight, B1500A) for the two p-Si/n-TiO_2 heterojunction devices fabricated using EBE and SG based TiO_2 TFs, respectively. The high frequency C-V measurements have been done to include only the depletion layer capacitance by avoiding the excess capacitance due to the interface states at low frequencies [Sze (1981), Chattopadhyay *et al.* (2001)]. The variations of the capacitance with applied bias in Figure 2.22 and Figure 2.23 clearly confirm the existence of a depletion region at the heterojunction interface. This demonstrates that the as fabricated diodes have a space charge region. Assuming an abrupt one sided n-TiO_2/p-Si heterojunction, the C-V characteristics of the n-TiO_2/p-Si heterojunction diode can be

described as [Werner and Güttler (1991), Somvanshi *et al.* (2014), Minemoto *et al.* (2015)]:

$$\frac{A^2}{C^2} = \frac{2(V_{bi} + V - kT/q)}{qN_D\varepsilon_s} \tag{2.6}$$

where, C is depletion capacitance, A ~0.785 × 10^{-2} cm^2 is the diode contact area, V is applied bias voltage, V_{bi} is the built in potential, N_D is the donor density or charge carrier concentration in n-TiO_2, q is electronic charge, ε_s is the dielectric constant of n-TiO_2, T is operating temperature, and k is Boltzmann's constant.

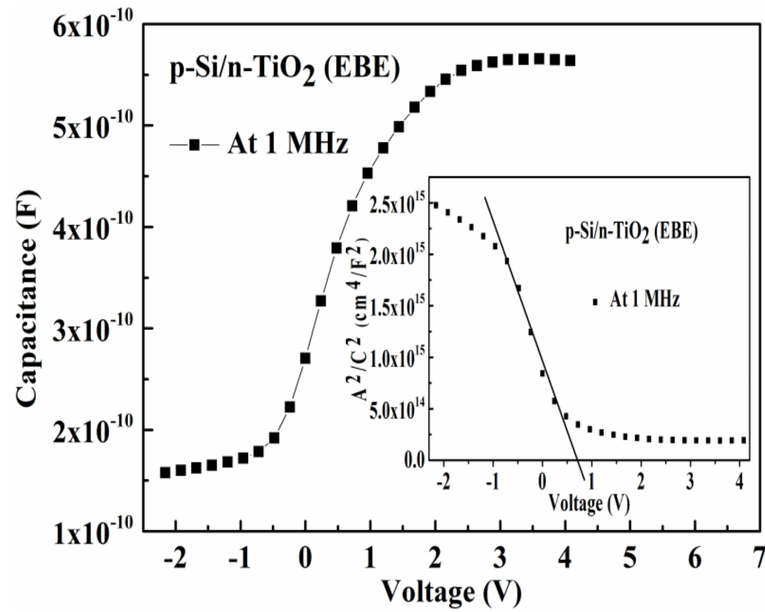

Figure 2.22: Forward bias C-V characteristics for n-TiO_2/p-Si heterojunction diode fabricated using EBE method. The inset figure illustrates its respective A^2/C^2 versus V plot.

Equation 2.6 demonstrates that the plot of A^2/C^2 versus V will be a linear curve whose intercept with the bias axis (V) gives the value of $-(V_{bi} - kT/q)$ while linear line slope (say, m) gives the doping concentration *(N_D)* of n-TiO_2:

$$N_D = \frac{2}{mq\varepsilon_s} \tag{2.7}$$

The A^2/C^2 versus applied voltage (V) curve can be used to obtain the built-in voltage (V_{bi}) by extrapolating the linear segment as shown in the insets of Figure 2.22 and Figure 2.23 for the EBE and SG TiO_2 film based heterojunction diodes, respectively. The estimated values of built-in potential for EBE and SG based devices are ~0.71 V and ~0.843 V, respectively. Now with the help of Eq. (2.7), the slope *(m)* of the linear section can be used to compute the carrier concentrations *(N_D)* in EBE and SG based TiO_2 TFs as ~1.0937×10^{16} cm^{-3} and 5.0811×10^{17} cm^{-3}, respectively.

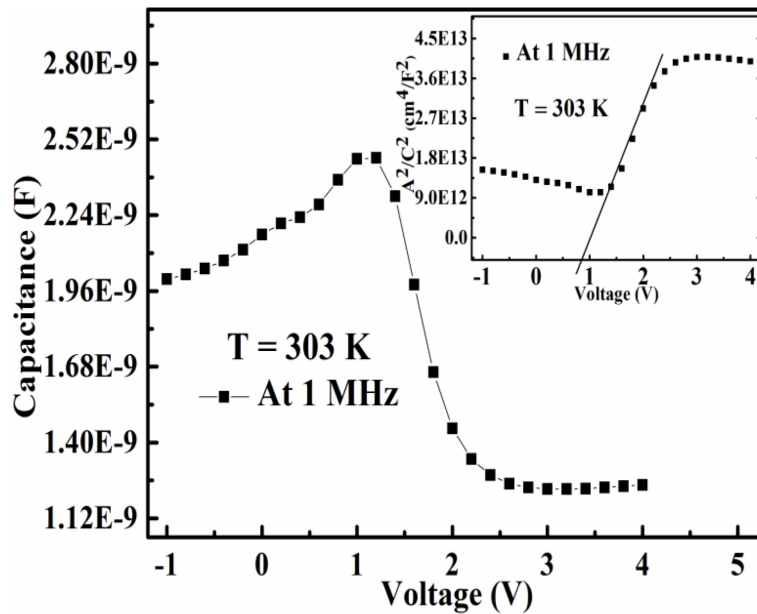

Figure 2.23: Reverse bias C-V characteristics for n-TiO_2/p-Si heterojunction diode fabricated using SG method. The inset figure illustrates its respective A^2/C^2 versus V plot.

The C-V characteristics can also be explored for estimating the value of barrier height $\left(\phi_{B,eff}^{\text{C-V}}\right)$ by the following relation [Chirakkara *et al.* (2012), Somvanshi *et al.* (2014)]:

$$\phi_{B,eff}^{\text{C-V}} = \mathrm{V_{d0}} + V_n \tag{2.8}$$

where, $V_{d0} = V_{bi} + \frac{kT}{q}$ represents the diffusion voltage at zero bias; and $V_n = \frac{kT}{q}\ln\left(\frac{N_C}{N_D}\right)$ is the depth of Fermi level below the conduction band in neutral region of the semiconductor where $N_C = 7.8 \times 10^{20}\ cm^{-3}$ is the effective density of states (DOS) in conduction band with $m^* = 10m_0$ as the effective mass of the electron for n-TiO_2 [Paracchino *et al.* (2012)].

The calculated barrier heights $\left(\phi_{B,eff}^{C\text{-}V}\right)$ for EBE and SG based heterojunction devices are obtained as ~1.029 eV and ~1.037 eV, respectively. Note that estimated values of barrier height and carrier concentration for the SG based heterojunction are larger than EBE based device. The results thus imply that we can obtain a better quality of p-Si/n-TiO_2 heterojunction by SG method than that achieved by using the EBE based film.

(c) Current-Voltage Characteristics of p-Si/n-TiO_2 TF Heterojunction Diodes Under Dark Condition

We will now discuss the measured Current-Voltage $(I - V)$ characteristics of the n-TiO_2 TF/p-Si heterojunction diodes fabricated via EBE and SG approach. The I-V characteristics are measured at ~295 K and in -12 V to +12 V bias range by using semiconductor device analyzer (Keysight, B1500A) under dark and UV illuminated conditions. Figure 2.24 compares the room temperature Current density vs. Voltage $(\ln J - V)$ characteristics of the n-TiO_2/p-Si heterojunction diode grown by using EBE and SG method. The inset of Figure 2.24 shows the schematic diagram of device structure. The as–fabricated heterojunction diodes show excellent rectifying behaviour with rectification ratio (i.e. the ratio (I_F / I_R) of the forward bias current at +12 V to the reverse bias current at -12 V) of ~237 and ~24520 corresponding to the EBE and SG TF

based heterojunction diodes, respectively. The value of rectification ratio for the SG TF based n-TiO_2/p-Si heterojunction diodes is much higher than the reported results of Refs. [Tsai *et al.* (2011), Selman *et al.* (2014), Sani (2014), Selman and Hassan (2015), Haider *et al.* (2015)]. The rectification ratio of two devices under study, have been compared and illustrated in Figure 2.25.

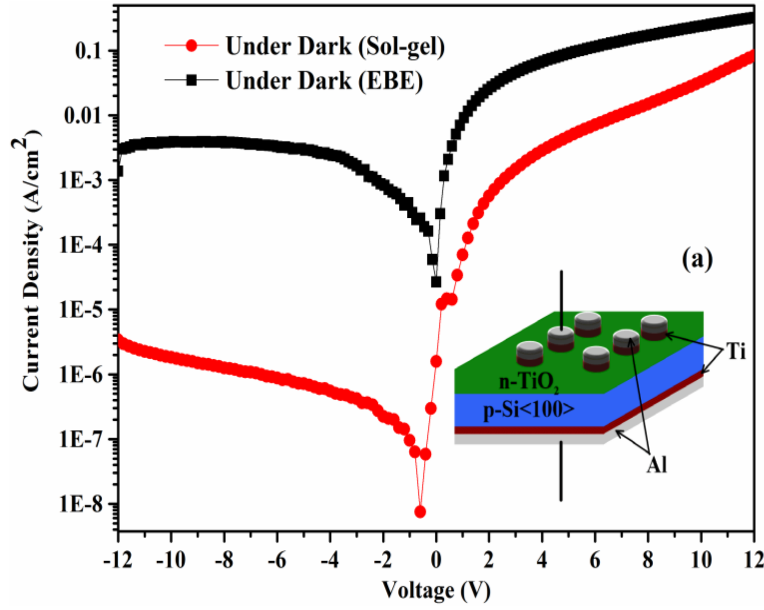

Figure 2.24: Comparative $\ln J - V$ characteristics of n-TiO_2/p-Si TF heterojunction diode under dark environment. The inset shows the schematic diagram of the Al/Ti/n-TiO_2/p-Si/Ti/Al device structure.

According to the thermionic emission theory, the $I - V$ characteristics of a heterojunction diode can be described as [Sze (1981), Zhang *et al.* (2012-a)]:

$$I = I_0 \left\{ \exp\left(\frac{qV}{\eta kT} \right) - 1 \right\} \tag{2.9}$$

$$I_0 = AA^* T^2 \exp\left(- \frac{q\phi_{B,eff}}{kT} \right) \tag{2.10}$$

where, q is the electronic charge, η is the ideality factor of the heterojunction, A $\approx 0.785\times10^{-2}$ cm^2 is the diode contact area, V is the bias voltage, I_0 is the reverse

saturation current, T is the absolute temperature, $A^* \approx 1200\ \mathrm{Acm^{-2}K^{-2}}$ $\left(\text{for}\ m_n^* = 10m_o\right)$ is the effective Richardson constant of TiO_2 [Zhang *et al.* (2012-a)], k is Boltzmann constant and $\phi_{B,eff}$ is the effective barrier height. By extrapolating the linear region of the $\ln(I)-V$ plot to zero bias-voltage as described in Ref. [Yadav *et al.* (2015)], the values of I_0 are estimated to be ~208.43 nA and ~12.212 nA for the EBE and SG TF based n-TiO_2/p-Si TF heterojunction diodes, respectively.

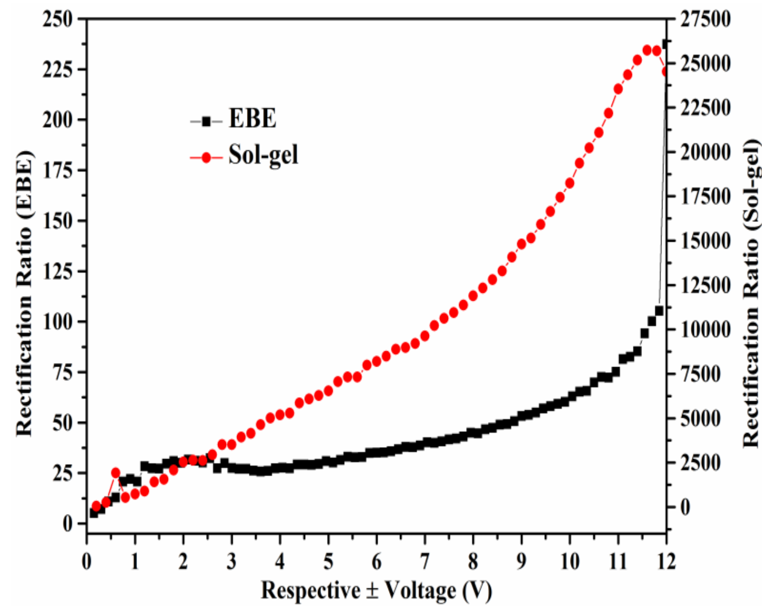

Figure 2.25: Comparative plot of rectification ratio versus respective bias voltage for the EBE and SG derived diodes.

The larger I_0 of EBE TF based heterojunction diodes than the SG TF based devices is attributed to the existence of large amount of oxygen vacancies on the surface of TiO_2 TFs [Xie *et al.* (2011)]. However, the estimated value of I_0 for the SG based device is much smaller than the reported values in the literature [Chinnamuthu *et al.* (2012), Selman *et al.* (2014), Sani (2014), Selman and Hassan (2015)]. The value of effective barrier height at zero bias can be computed using given relation [Hazra *et al.* (2014-c)]:

$$\phi_{B,eff} = \left(\frac{kT}{q}\right)\ln\left(\frac{AA^{*}T^{2}}{I_{0}}\right) \tag{2.11}$$

By putting value of I_0 in Eq. (2.11), the values of $\phi_{B,eff}$ are calculated as ~0.7383 eV and ~0.8105 eV for the EBE and SG based devices, respectively. These estimated values using I-V measurement are very close to the theoretical value defined as the difference between the work functions of Si and TiO_2 [Romero *et al.* (2004)]. It is important to note that the barrier heights estimated from the I–V and C–V characteristics are in similar trend. Although some difference between estimated barrier heights using I–V and C–V characteristics may be attributed to the edge-leakage current and image force-induced barrier lowering as observed in Ref. [Zhang *et al.* (2014)].

The ideality factor (η) for two types of heterojunction devices under study can be given by [Sze (1981)]:

$$\eta = \left(\frac{q}{kT}\right)\left\{\frac{dV}{d(\ln I)}\right\} \tag{2.12}$$

The calculated values are η ~3.1466 and η ~3.8388 for the EBE and SG based heterojunctions, respectively which are closely consistent with the observations reported in Refs. [Liu *et al.* (2012-b), Chakrabartty *et al.* (2014), Somvanshi *et al.* (2014)]. The above calculated diodes parameters under dark condition are listed in Table 2.3.

Table 2.3: Parameters of Si/TiO_2 heterojunction diode Under Dark condition.

Parameters	**SG Based Device**	**EBE Based Device**
On/off ratio at ±12 V (Rectification ratio)	24520	237
Saturation current (nA)	12.212	208.43
Ideality factor (η)	3.8388	3.1466
Barrier height (eV)	0.8105	0.7383

(d) Current-Voltage Characteristics of p-Si/n-TiO$_2$ TF Heterojunction UV Photodiodes

The UV source (make: Benchmark, India) is used for the photoresponse measurement of the heterojunction diodes under consideration and has an output optical power of 650 μW (measured by a power meter of Model No.: FOMP-101, Benchmark, India) at 365 nm wavelength. Now in Figure 2.26 we have compared the $\ln J - V$ characteristics of the two n-TiO$_2$ TF/p-Si heterojunction diodes under dark and UV illumination conditions. The large changes in the reverse bias currents due to the incident UV light suggest that both the diodes are suitable for UV detection applications. The contrast ratio (i.e. the ratio of the photocurrent (I_{ph}) to the dark current (I_d) at a particular bias voltage) of the photodiodes under consideration is calculated as ~14.92 and ~56704.8 at -10 V bias for the EBE and SG based n-TiO$_2$/p-Si heterojunction photodiodes, respectively. In Figure 2.27 the contrast ratio of two devices under study, have been compared over the voltage range from -12 V to +12 V. The maximum value ~83911 of the contrast ratio at -5.2 V bias of the SG TF based heterojunction photodiode is much better than other reported TiO$_2$ TF based heterojunction diodes [Tsai *et al.* (2011), Selman *et al.* (2014), Sani (2014), Selman *et al.* (2015)]. Further, the maximum value of the contrast ratio of the SG based heterojunction photodiode is observed to be ~6445 times larger than that of the EBE based heterojunction device at the same reverse bias voltage of -5.2 V. Thus, the superior rectification ratio and contrast ratio of the SG derived n-TiO$_2$ TF based heterojunction photodiode make it a better choice for the UV detection applications over the EBE based device.

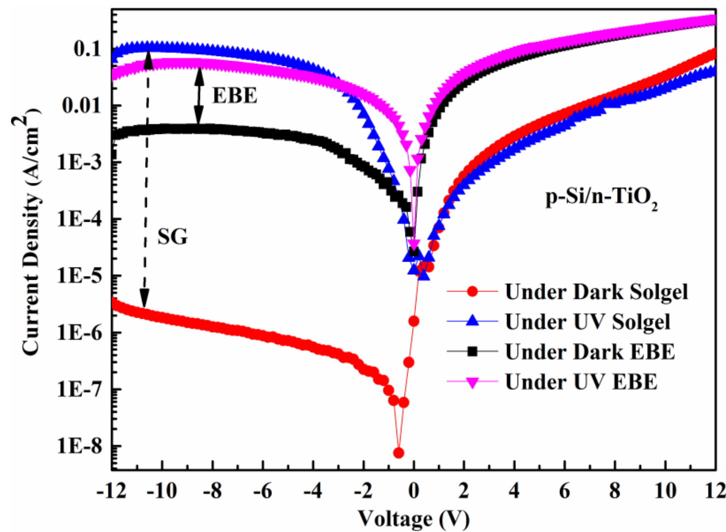

Figure 2.26: Comparative $\ln J - V$ characteristics of n-TiO_2/p-Si heterojunction photodiodes under dark and UV environment for the EBE and SG derived TFs.

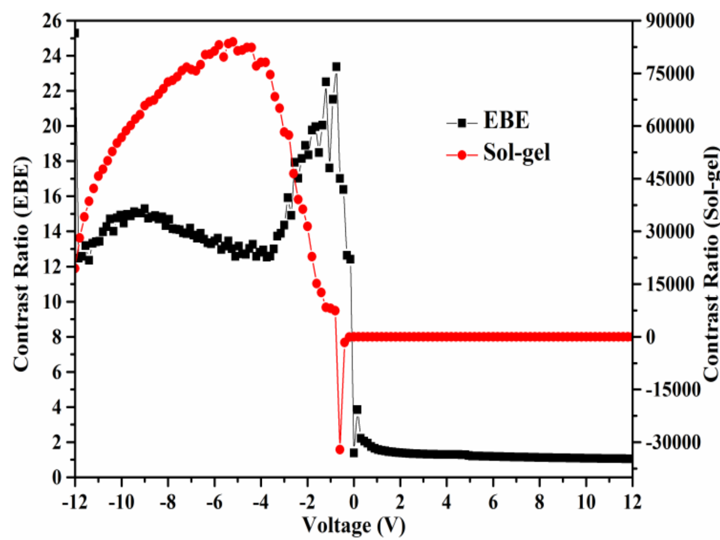

Figure 2.27: Comparative plot of contrast ratio versus bias voltage for the EBE and SG derived photodiodes.

Besides the rectification ratio and contrast ratio, we now estimate other performance defining parameters such as the responsivity (R_{UV}), Gain, bias dependent specific detectivity (D), and the resistance-area products (RA) of the EBE and SG derived TiO_2 TF based n-TiO_2/p-Si heterojunction photodiodes. The responsivity is given by [Sze (1981)]:

$$R_{UV} = \frac{I_{ph}}{P_{opt}} \tag{2.13}$$

where, I_{ph} is the photocurrent and P_{opt} is the incident optical power. The values of R_{UV} are calculated as ~0.693 A/W and ~1.247 A/W at a bias voltage of -10 V for EBE and SG TF based heterojunction diodes, respectively. The responsivity of the SG TF based n-TiO_2/p-Si heterojunction photodiode is not only much larger than that of the EBE TF based heterojunction under study but also much better than the previously reported results in the literature [Selman *et al.* (2014), Chakrabartty *et al.* (2014), Sani (2014), Selman and Hassan (2015)]. The enhanced responsivity in the SG based photodiodes was attributed to the modification of oxygen species adsorbed at the surface of the TiO_2 TFs under illumination and trapped incident photons [Xie *et al.* (2011), Selman *et al.* (2014)]. The higher responsivity of the SG based device may also indicate the existence of an internal photoconductive gain induced by the desorption of oxygen on the TiO_2 surface [Xie *et al.* (2011)].

The photoconductive gain *(g)* can be given as [Soci *et al.* (2007), Huang *et al.* (2010)]:

$$g = \frac{1240 \times R_{UV}}{\lambda(nm) \times EQE} \tag{2.14}$$

where, EQE is external quantum efficiency and $\lambda(nm)$ is the wavelength in nm of the incident UV light. Assuming $EQE = 1$ [Soci *et al.* (2007)], the gain is calculated as ~2.35 and ~4.24 for the EBE and SG device, respectively. Our estimated gain for the SG based device is higher than reported in literature Ref. [Selman *et al.* (2014)]. Now, using the Eq. (2.13), we can estimate the voltage dependent detectivity (D) of the heterojunction photodiodes by using the following equation [Yadav *et al.* (2015)]:

$$D = R_{UV}\left(\frac{RA}{4kT}\right)^{1/2} \tag{2.15}$$

where, RA is the resistance-area product of the detector which can be obtained from the $J-V$ characteristics as [Hazra *et al.* (2014-c)]: $RA=(dJ/dV)^{-1}$. From the $J-V$ characteristics, the values of RA and D are obtained as RA ≈255.98 Ω.m^2 and D ≈8.62×10^{10} mHz$^{1/2}$W^{-1} for the EBE based n-TiO_2/p-Si heterojunction photodiode and RA ≈279.26 Ω.m^2 and D ≈1.62×10^{11} mHz$^{1/2}$W^{-1} for the SG TF based n-TiO_2/p-Si photodiode at -10 V bias voltage. Our calculated detectivity (D) for both fabricated TFs is better than as reported by Mazhir *et al.* [Mazhir *et al.* (2015)]. The zero-bias resistance-area product (R_0A) values for the two devices under consideration are ~132.88 Ω.m^2 and ~20639.16 Ω.m^2 for the EBE and SG based heterojunctions, respectively. It is clearly observed that SG derived TiO_2 TFs are better material for the n-TiO_2/p-Si UV photodiode applications than the EBE based TiO_2 TFs. The estimated UV detection parameters for two photodiodes under study are summarized in Table 2.4.

Table 2.4: Comparison of the UV photo detection parameters for two p-Si/n-TiO_2 heterojunction photodiodes under study.

UV wavelength	365 nm	
Power of incident light	650 μW	
Operating Voltage	-10 V	
Parameters	**SG Device**	**EBE Device**
Contrast ratio	56704.8	14.92
Responsivity [A/W]	1.247	0.693
Detectivity [mHz$^{1/2}$W^{-1}]	1.62×10^{11}	8.62×10^{10}
Gain	4.24	2.35
RA products [Ω.m^2]	279.26	255.98
R_0A [Ω.m^2]	20639.16	132.88

2.4.5 Time Response Characteristics

In this section, we will investigate the transient response characteristics of the two types of p-Si/n-TiO_2 heterojunctions under study. For the time response measurements, we have used a digital multimeter (Agilent, 34410A) and an UV LED source with ON-OFF light pulse duration of 1 sec. each. The ON-OFF pulsating light is obtained by using Arduino™ microcontroller and the digital multimeter is controlled by LabView™. The UV LED source has central frequency at ~390 nm with optical power density of ~3.50 mW/cm^2 (measured by PM100D). The measured results (observed at -1 V DC bias) are plotted between time (in sec.) and current (A) and shown in Figure 2.28 (a) and (b).

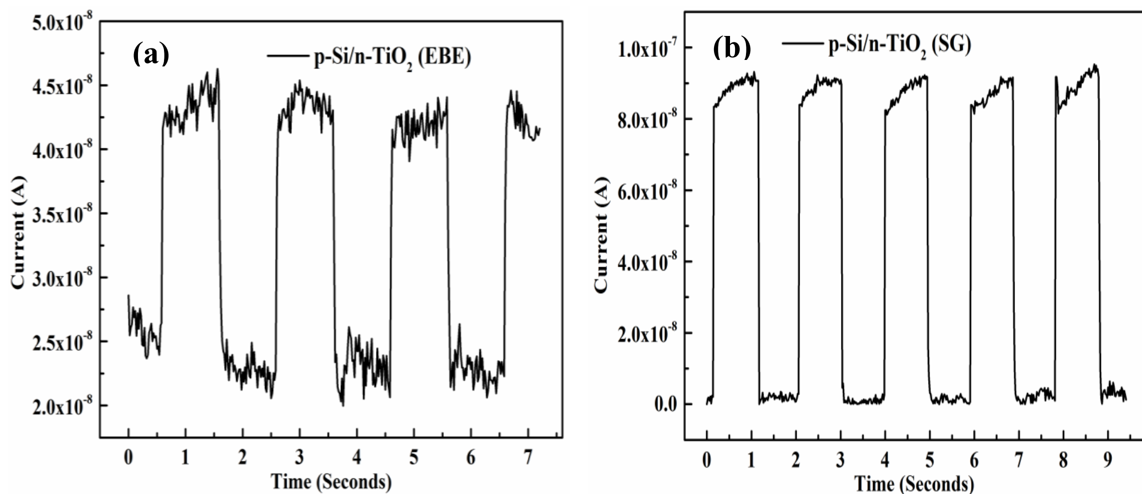

Figure 2.28: Current vs Time characteristics of the heterojunction PDs under dark and UV environment for (a) EBE and (b) SG derived TFs.

Since photodiodes are operated in reverse bias, their time response characteristics can be correlated to the minority carrier mobility of the photodiodes [Pearsall (2003)]. At a fixed -1 V DC bias the estimated average response (rise) time and recovery (fall) time are ~33.81 ms and ~46.06 ms, respectively for EBE TiO_2 film based heterojunction whereas the corresponding values for the SG based devices are ~16.28 ms and ~25.88

ms. The faster response and recovery times of the SG based p-Si/n-TiO_2 heterojunction can be attributed to the better quality of TiO_2 films than that of the EBE based films. The time response of the SG based heterojunction is also better than p-Si/n-TiO_2 heterojunction devices reported by others [Xie *et al.* (2013), Sani (2014), Selman and Hassan (2015)].

2.4.6 Energy Band Diagram

Now, we will investigate the possible UV detection mechanism for the two devices. Note that the operation of both the n-TiO_2/p-Si heterojunction diodes under UV illumination involves basically three steps: (1) the generation of electron–hole pairs by absorbing incident photons with energy $(h\upsilon)$ greater than the band gap of TiO_2; (2) the separation and transport of electron–hole pairs by the internal electric field in the depletion region; and (3) the interaction of current with the external circuit to generate an output signal i.e (I_{ph}) [Sze (1981), Selman *et al.* (2014)].

The operation of the p-Si/n-TiO_2 heterojunction photodiodes under consideration has been demonstrated in Figure 2.29 through a generalized energy band diagram of the device under UV illumination and reverse bias operation. Assuming the respective values of the electron affinities of n-TiO_2 and p-Si as ~4.1 eV [Chen *et al.* (2015)] and ~4.05 eV [Somvanshi and Jit (2014)]; and the energy bandgaps of TiO_2 and Si as $E_{g,TiO_2} \sim 3.3\,\text{eV}$ and $E_{g,Si} \sim 1.12\,\text{eV}$, the conduction band offset and valence band offset can be calculated using the Anderson's model [Sze (1981), Somvanshi and Jit (2014)] as $\Delta E_C = \chi_{TiO_2} - \chi_{Si} = 0.05\,\text{eV}$ and $\Delta E_V = E_{g,TiO_2} - E_{g,Si} + \Delta E_C = 2.23\,\text{eV}$, respectively. Since the p-Si substrate is considered to be moderately doped and device is operated for UV detection under the reverse bias condition, the depletion region can be

expected to be extended mainly into the intrinsic n-TiO_2 film and hence the entire TiO_2 film of thickness ~120 nm can be assumed to be fully depleted.

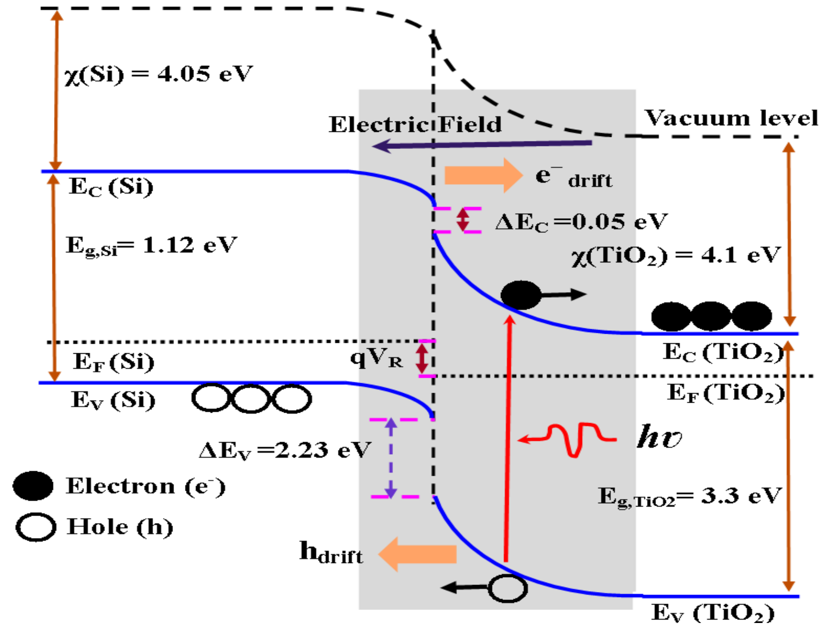

Figure 2.29: Schematic energy-band diagrams of p-Si/n-TiO_2 heterojunction diode under UV illumination using Anderson's model.

Further, it may also be mentioned that the absorption coefficient of most of the semiconductors is very high (~10^5 cm^{-1}) in the UV region which results in an effective absorption length of ~100 nm or less [Sze (1981)] in TiO_2 film. Thus, the photocurrent in the present device is a result of the excess electron-hole pair generation due to the UV light absorption mainly in the depletion region of the n-TiO_2 film as shown in the Figure 2.29. Whenever an electron-hole pair is generated due to the absorption of a photon with energy $\geq E_{g,TiO_2}$ in the TiO_2 film, the photo-generated electron in the conduction band is drifted out in the opposite direction to the electric field whereas the photo-generated hole in the valence band is drifted in the same direction of the electric filed present in the depletion region as shown in the Figure 2.29. The large electric filed

under reverse bias results in an enhanced photocurrent in the devices under consideration.

2.5 Summary and Conclusion

In this chapter after fabrication, the morphological, structural, electrical and optical properties of n-TiO_2 TFs deposited on p-Si substrates by using the EBE and SG with spin coating methods have been compared for investigating their suitability for UV detection applications. The structural and optical characterization of as grown TiO_2 TFs have been analyzed by HRSEM images, AFM images, XRD analysis, EDAX, UV-Vis spectrum, reflectance, transmittance spectrums, and PL spectroscopy measurements. From the absorption spectra of EBE and SG deposited films, the band gap of EBE and SG based TiO_2 TFs are obtained as ~3.1 eV and ~3.3 eV, respectively. The as-fabricated n-TiO_2/p-Si heterojunctions using EBE and SG based TiO_2 TFs have excellent rectifying and UV detection characteristics with respective rectification ratio of ~65 and ~18240 and the contrast ratio of ~14.9 and ~56704 at 10 V bias. The barrier height, ideality factor, responsivity, photoconductive gain, specific detectivity and resistance-area product measured for the EBE and SG based heterojunction photodiodes under consideration are ~0.7383 eV, ~3.1466, ~0.693 A/W, ~2.35, 8.62×10^{10} $mHz^{1/2}W^{-1}$ and ~132.88 $\Omega.m^2$; and ~0.8105 eV, ~3.8388, ~1.25 A/W, ~4.24, ~1.62×10^{11} $mHz^{1/2}W^{-1}$ and ~20639.16 $\Omega.m^2$, respectively at 10 V bias. The ~223.74 times enhancement in the rectification ratio, ~6445 times in the contrast ratio (at -5.2 V) and about 2 times larger responsivity of the SG based n-TiO_2/p-Si heterojunction diodes suggest their superiority for UV detection applications over the EBE TiO_2 TF based n-TiO_2/p-Si heterojunctions. The above conclusion is also supported by the larger values of the barrier height, specific detectivity, external quantum efficiency and resistance-area product of the SG

based n-TiO_2/p-Si heterojunction photodiodes than the EBE based devices. Further the response and recovery time for EBE based photodiode is ~33.81 ms and ~46.06 ms whereas in case of SG based photodiode it is ~16.28 ms and ~25.88 ms. Finally, the energy band diagram was analyzed using Anderson model. The result shows that fabrication technique also plays very significant role in the device performance.